

Far-Infrared Galaxies in the Far-Ultraviolet¹

Jeffrey D. Goldader

Department of Physics and Astronomy, University of Pennsylvania, Philadelphia, PA 19104

jdgoldad@dept.physics.upenn.edu

Gerhardt Meurer, Timothy M. Heckman, Mark Seibert

The Johns Hopkins University, Baltimore, MD 21218

D. B. Sanders

Institute for Astronomy, University of Hawaii, 2680 Woodlawn Drive, Honolulu, HI 96822

Daniela Calzetti

Space Telescope Science Institute, Baltimore, MD 21218

Charles C. Steidel

Palomar Observatory, California Institute of Technology, Pasadena, CA 91125

ABSTRACT

In an effort to better understand the UV properties of ultraluminous infrared galaxies (ULIGs), and compare them to the rest-frame UV properties of high redshift sub-mm and Lyman-break galaxies, we have obtained far- and near-UV imaging observations ($\lambda_{eff} = 1457\text{\AA}$, $\lambda_{eff} = 2364\text{\AA}$, respectively) of two luminous infrared galaxies (LIGs—VV 114 and IC 883) and five ULIGs (IRAS 08572+3915, Mrk 273, IRAS 15250+3609, Arp 220, and IRAS 19254–7245) using the Hubble Space Telescope. All the galaxies were detected in both channels. UV light, both diffuse and from star clusters, can be traced to within the inner kpc of the dominant near-IR nuclei. However, in general, the brightest UV sources are clearly displaced from the *I*-band and near-IR peaks by at least hundreds of pc. Further, only 0.07%–7.3% of the total near-UV light is projected within the inner 500 pc radius, even though this is the same region wherein most of the bolometric energy is generated. All nuclei are highly obscured by dust. Even after correction for dust reddening, the global UV emission fails to account for the total bolometric luminosities of these systems by factors of 3–75.

The discrepancy is much worse if only the central regions, where the bolometric luminosities are generated, are included. In two cases (VV 114 and IRAS 08572+3915), the merging companion galaxies are more prominent in the UV than the more IR-luminous member. While all our galaxies show possible signatures of AGN activity, only IRAS 19254–7245 yields even a possible detection of an AGN in our UV images. Simple calculations show that all but one of our galaxies would be expected to drop below the detection thresholds of, e.g., the Hubble Deep Fields at redshifts between 1.5 and 3, and we find that ~ 2 of our 5 ULIGs would be selected as Extremely Red Objects in this redshift range. A typical ULIG in our sample would be too faint to be detected at high-redshift in the deepest current optical or sub-mm deep surveys. Only VV 114 has UV luminosity and color similar to Lyman-break galaxies at $z \sim 3$; the other galaxies would be too faint and/or red to be selected by current surveys. The low UV brightnesses of our ULIGs mean that they would not appear as optically-bright (or bright ERO) sub-mm galaxy counterparts, though they might be similar to the fainter sub-mm galaxy counterparts.

1. Introduction

A significant challenge in astronomy today is understanding the relationships between very distant galaxies and nearby galaxies. Recent observations have identified many luminous, high-redshift systems, yet they are faint and very difficult to study in detail. Are there good local counterparts for these galaxies? If so, we may try and use the local counterparts to better understand their distant relatives.

New observations, carried out primarily with the Sub-millimeter Common User Bolometer Array (SCUBA: Holland et al. 1999) on the James Clerk Maxwell Telescope, have revealed the presence of a significant population of far-IR (FIR) luminous galaxies, most likely at redshifts $z \gtrsim 2$ (“sub-mm galaxies,” e.g., Smail et al. 1998, Barger et al. 1999a). These galaxies are apparently responsible for much of the FIR and sub-mm extragalactic background radiation, whose energy density is comparable to that of the integrated optical light of faint galaxies seen in, e.g., the Hubble Deep Fields (HDFs) (e.g., Hauser et al. 1998; Barger, Cowie & Sanders 1999). The sub-mm galaxies detected to date are much more lu-

¹Based on observations with the NASA/ESA Hubble Space Telescope obtained at the Space Telescope Science Institute, which is operated by the Association of Universities for Research in Astronomy, Incorporated, under NASA contract NAS5-26555.

minous than almost any galaxy in the local universe. It is possible that a significant fraction of the star formation in the early universe occurred in FIR-luminous galaxies, of which the current sample of sub-mm galaxies are the most luminous. At present, it is not clear if the sub-mm galaxies are at all related to galaxies at similar redshifts discovered by the Lyman break technique, even though the brightest, reddest Lyman break galaxies (LBGs) may have comparable bolometric luminosities, after reddening is taken into account (Meurer et al. 1999; Adelberger & Steidel 2000). Most (but not all) sub-mm galaxies are too faint and/or red to be found with LBG selection criteria.

For the sub-mm galaxies with known redshifts, the bluest sub-mm observations (at, e.g., 450 μm) still fall on the Rayleigh-Jeans side of the rest-frame FIR peak wavelengths. Nonetheless, the limited information on these sub-mm galaxies shows that they appear to have overall rest-frame FIR/radio spectral energy distributions quite similar to those of the ultraluminous infrared galaxies discovered in the local universe ($z \lesssim 0.1$). This has led to increased interest in the nearby infrared galaxies as possible counterparts.

Ultraluminous infrared galaxies ² (ULIGs, with $L_{IR} > 10^{12}L_\odot$) were found to be a significant class of objects upon analysis of the Infrared Astronomical Satellite (IRAS) all-sky survey (Soifer et al. 1987; Sanders et al. 1988). The bolometric luminosities of ULIGs, the most powerful infrared-luminous galaxies, are similar to those of optically-selected quasars. We now understand ULIGs to be a stage in the merger of two gas-rich spiral galaxies. During the merger, the molecular gas is driven inward towards the nuclei, where the gas serves to fuel a tremendous burst of star formation and, perhaps, AGN activity as well. Dust absorbs and re-radiates the light from young stars and/or the AGN. Complicating our understanding of ULIGs is the fact that most of the energetic activity takes place in the inner few hundred pc, where small angular sizes and almost entirely opaque ISM prevent us from directly witnessing events occurring in the nuclei themselves.

The primary goal of our study is to explore the possible connection between sub-mm galaxies and ULIGs. There is substantial circumstantial evidence linking ULIGs and sub-mm galaxies, but a direct connection has not been established. In part, this is because of observational considerations. The FIR/radio spectral energy distributions (SEDs) of the best-studied sub-mm galaxies (ERO J164502+4626.4: Dey et al. 1999; SMM J02399–0136: Ivison et al. 1998; SMM J14011+0252: Ivison et al. 2000; and SMM J02399–0134: Barger et al. 1999a) are sampled redward of the rest-frame FIR peak, which should occur at 60–100 μm if their dust temperatures are similar to those of the ULIGs. Optical and near-IR

²See Sanders & Mirabel (1996) for a review. $L_{IR} = L(8 - 1000\mu\text{m})$, computed using the prescription in that paper.

observations sample blueward of $\sim 0.6 \mu\text{m}$ in the rest-frame for $z \sim 2.5$. As a result, we know little or nothing of the properties of sub-mm galaxies from the red optical through $\sim 200 \mu\text{m}$ in the rest-frame. And unfortunately, local ULIGs are poorly studied shortward of $\sim 4000 \text{\AA}$. What morphological comparisons we can make using, e.g., optical images, are quite limited. As a result, the strongest links between ULIGs and sub-mm galaxies are made largely on the basis of three facts. First, ULIGs and sub-mm galaxies are the most highly luminous systems in the far-IR in the local universe and at $z \gtrsim 1$ respectively, although most sub-mm galaxies detected so far are inferred to be still a factor of few more luminous than ULIGS such as Arp 220 (Barger, Cowie & Richards 2000). Second, ULIGs and sub-mm galaxies also have similar far-IR/sub-mm/radio SEDs. Finally, large amounts of molecular gas (e.g., CO) have been detected in both classes of objects.

Local counterparts, even when not exact matches, can offer important insights on high- z systems. For example, starbursts observed with IUE (e.g., Meurer et al. 1999 and references therein) have SEDs and UV spectral properties like LBGs, though the local galaxies are smaller and less luminous; this has been used to infer that the basic physics (e.g., winds, reddening) of these objects are similar. We hope that observations of ULIGs in the rest-frame UV, telling us about their morphologies, luminosities, and colors, might both allow a test of their fitness as counterparts of sub-mm galaxies, and also allow us to better interpret the rest-frame UV observations of sub-mm galaxies.

A secondary goal is to test whether ULIGs follow what is known as the “IRX- β ” correlation between the redness of the UV continuum (parameterized by the UV spectral slope β between $\sim 1600 \text{\AA}$ and 2200\AA , where $f_\lambda \propto \lambda^\beta$) and the IR-excess (the IRX, defined as the ratio of the FIR/UV fluxes³), that has been established for a sample of local starbursts observed in the UV (Meurer et al. 1995, 1997, 1999). The correlation is well fit by a foreground dust shell model, wherein dust surrounding the UV-bright region both reddens and absorbs the UV light, reprocessing it to FIR wavelengths. The correlation appears to hold for $L \lesssim 10^{11.5} L_\odot$, but has not been tested at higher luminosities. If ULIGs also follow this correlation, then we would have more confidence that rest-frame UV observations of even the most dusty high- z star-forming galaxies can be used to estimate their total bolometric luminosities (dominated by the difficult to access far-infrared) ensuring that these galaxies are included in the census of star formation in the early universe. We know that β and the

³In this paper, we compute the FIR fluxes according to the prescription of Helou et al. 1988, including the dust temperature dependent color correction factor defined in the appendix of that paper. We note that Meurer et al. use a constant color correction factor reasonable for the typical dust temperatures of their galaxies. The UV flux is computed as $F_\lambda = \lambda \times f_\lambda$ in the FUV channel, where f_λ is the observed flux density in $\text{erg/cm}^2/\text{s}/\text{\AA}$.

IRX correlate with total luminosity for the Meurer et al. sample (Heckman et al. 1998). If these trends hold at higher L and higher z , then sub-mm galaxies may be too red to be selected as LBGs, and may perhaps better be associated with Extremely Red Objects (e.g. Ivison et al. 2000, ApJ, 542, 27).

In this paper, we present new rest-frame UV observations of seven galaxies with $L_{IR} > 10^{11.5}$. Three ULIGs (VII Zw 31, IRAS 12112+0305, and IRAS 22491–1808) were detected in the UV using the Faint Object Camera on the pre-COSTAR Hubble Space Telescope (HST) by Trentham, Kormendy, & Sanders (1999, hereafter TKS). Though their photometric precision was limited by the spherical aberration and high backgrounds, the detections were good evidence that our program was in fact feasible. More recently, ground-based images in the U' band ($\lambda = 3410\text{\AA}$, $\Delta\lambda = 320\text{\AA}$) were obtained for many ULIGs (including three of our galaxies, IRAS 08572+3915, Mrk 273, and IRAS 15250+3609, plus two galaxies, IRAS 12112+0305 and IRAS 22491–1808, from TKS) by Surace & Sanders (2000).

This paper concentrates on the large-scale photometric and morphological properties for the galaxies in our sample. We will first describe the observations and data reduction procedures. Then, we comment on the UV photometric properties of the galaxies (e.g., IRX- β). We give detailed descriptions of each system, then discuss their detectability at high- z . Finally, we consider our systems in relation to Lyman-break galaxies, extremely red objects, and sub-mm galaxies. Here, we assume a Hubble Constant of $H_0 = 70 \text{ km/s/Mpc}$, with $\Omega_M = 0.3$ and $\Omega_\Lambda = 0.7$. Computing angular size and luminosity distances in a cosmology with nonzero Λ is described by Carroll, Press & Turner (1992).

2. Observations

We constructed a flux- and luminosity-limited sample of luminous infrared galaxies (LIGS: $L_{IR} = 10^{11} - 10^{12}L_\odot$) and ULIGs from the IRAS Bright Galaxy Sample, then selected from that list seven relatively nearby galaxies that had already been imaged at other wavelengths by HST. Our sample spans a factor of 4 in IR luminosity, including 2 LIGs at the highest luminosities of the starbursts studied in the papers by Meurer et al., $4 \times 10^{11}L_\odot$, and 5 ULIGs, going up to $1.5 \times 10^{12}L_\odot$ (listed in order of increasing right ascension in Table 1).

We obtained our far- and near-UV images using the MAMA detectors of the Space Telescope Imaging Spectrograph (STIS) on HST. In the near-UV channel (STIS NUV-MAMA+F25QTZ filter, $\lambda_{pivot} = 2364\text{\AA}$, $\Delta\lambda = 903\text{\AA}$ FWHM), we obtained two exposures totalling 1500 seconds, with the telescope offset by $0''.24$ in RA and DEC between exposures.

The far-UV observations (STIS FUV-MAMA+F25SRF2 filter, $\lambda_{pivot} = 1457\text{\AA}$, $\Delta\lambda = 244\text{\AA}$ FWHM), were divided into 2–3 similarly offset pairs of images, for far-UV exposure times of 2829–3891 seconds. Details of the exposures are given in Table 2.

3. Analysis

We analyzed the STScI pipeline-processed STIS data as follows. First, we split the paired far-UV images into single ones, giving typically six far-UV images and two near-UV images per galaxy. For each individual image, we determined and subtracted the mean values of the sky found from large regions well away from detectable galaxy emission. The far-UV background was found to vary significantly in some cases, due to light near the limb of the Earth. Because the extended emission from our sources is typically 1–2 DN per pixel, a few images with high backgrounds ($> 1 - 2$ DN per pixel) were rejected, because the S/N ratios of the combined images would have been limited by the Poisson noise of the high-sky images. The images were aligned and co-added using the DRIZZLE package in IRAF (v2.10), with which we also corrected the geometric distortion (using the cubic distortion coefficients from the STIS Instrument Handbook, Version 3, June, 1999) and rotated the images to the standard North-up, East-left orientation. We also magnified the far-UV images to the same platescale as the near-UV images ($0''.024465/\text{pixel}$) during the DRIZZLE process.

For the STIS images, determining accurate sky values was important because much of the total UV flux comes from large regions with surface brightnesses near the residual sky levels. The uncertainty in our photometry is therefore quite sensitive to accurate subtraction of the residual sky levels. We measured the sky counts in the darkest regions of the images, in a few contiguous groups of 20×20 pixel boxes, about 30–40 boxes in total for each final UV image. We determined the residual sky levels for each of the final images from the averages of the means of the sky counts in the boxes, and the uncertainties in the residual sky levels were set to the 1σ scatter in the means of the sky counts of the boxes. One galaxy, Arp 220, was especially problematic, because its large angular size resulted in faint emission essentially filling the entire STIS field of view. For Arp 220, the darkest regions of the UV images turned out to be located within the dark dust lanes apparent in optical images.⁴ In

⁴For Arp 220, the raw NUV sky values are heavily quantized at around 0 and 1 DN/pixel. The mean values of the raw NUV skies in large, dark areas of the images, in these 750 second exposures, were ~ 0.1 DN/pixel. The FUV sky means, in large sections of the raw UV images, varied from 0.004 DN/pixel to 0.68 DN/pixel from image to image. The variation was due to scattered light from near Earth’s limb in the images. So, the highest the true FUV (sky+galaxy) value could have been was 0.004 DN/pixel, in an exposure of 690 seconds. Any extended emission from the galaxy can have at most that much flux. After

all other galaxies, comparison with WFPC2 (or NICMOS) images show that the STIS field of view was large enough that we should have regions of blank sky in our STIS images, and those regions with lowest counts were used to determine the sky levels.

Measuring total fluxes is difficult because the objects have irregular shapes, and in several cases their surface brightnesses barely ever reach above the sky level over much of the face of the galaxy. We developed a “buffered isophote” technique for measuring total fluxes. First, we used the adaptive smoothing algorithm of Scoville et al. (2000) to make a smoothed FUV image of each galaxy. This was used to make a “good pixel” mask of all pixels in the smoothed image that are $\geq 3\sigma$ above the background, where σ is the scatter about the mean background as described above. It is important to use the smoothed image for this so that the fluxes are not biased upwards by positive noise deviations. Since the light distribution undoubtedly extends beyond the 3σ isophote, we then buffered this mask by appending all pixels within $1''$ of the previously marked pixels as also being “good.” The choice of $1''$ as the buffer size is somewhat arbitrary, but by blinking the mask and the smoothed images it was clear that there is little or no real structure beyond the mask. The total flux is then found by adding the flux in the “good” pixels of *the original images* (before smoothing). Both the FUV and NUV fluxes were extracted with the FUV mask. Using the NUV image to create the mask often resulted in slightly larger fluxes, but the differences were within the photometric errors. We also performed simple circular aperture photometry in apertures of 0.5, 1, 2, 3, and 5 kpc physical radius in our assumed cosmology (Table 3). We note that the larger apertures can include flux from companion or field galaxies in some cases. Errors were determined from photon statistics and the uncertainties in the sky levels (the latter dominates in all cases). In all but one case (IRAS 19254–7245), at least 85% of the “total” flux is contained within the 5 kpc radius aperture (or the sum of the two apertures for IRAS 08572+3915 and VV 114). We note that photometry of IRAS 19254–7245 in large apertures is intrinsically uncertain at the level of 0.26–0.46 magnitudes because of the very low flux levels, and some of the “missed” flux likely comes from a few star clusters outside the 5 kpc apertures.

WFPC2 images of the five of our galaxies with $L_{IR} > 10^{12}L_\odot$ had been taken, and we retrieved those from the HST Archive. We co-added the pipeline-calibrated images, using CRREJ and COSMICRAYS to correct for cosmic rays and hot pixels. We then used DRIZZLE to perform the geometric corrections, adjust the pixel scale to that of the STIS

combining the FUV images with those sky values subtracted, the final value of the FUV “residual” sky was $< 1\sigma$ from zero. Our error estimates should adequately incorporate the possibility of errors in the sky determination. In short, the extremely low counts in dark areas of the raw Arp 220 UV images lead us to believe that we are not losing significant amounts of uniform, extended light across the images.

images, and rotate the images to the standard North-up orientation.

NICMOS images of all but one of our galaxies (IRAS 19254–7245) were taken and made available in reduced form by Scoville et al. (2000). We used MAGNIFY and ROTATE to set the pixel scale and orientation to those of the STIS images. In all cases, there were enough common details between the UV and optical, and near-IR and optical, that we could confidently co-register the multi-wavelength data relative to the WFPC2 images using IMSHIFT. (For the two galaxies without WFPC2 images, VV 114 and IC 883, we aligned the UV and IR images relative to the F110W and F160W images.) We estimate registration uncertainties of $\lesssim 1$ STIS pixel.

4. Results

4.1. Global UV properties

4.1.1. The relationship between UV color and the FIR/UV excess

As noted in Section 1, Meurer et al. (1999) (hereafter M99) describe an empirical relationship between the color of the UV continuum (parameterized by β) and the FIR/UV flux ratio for a sample of starbursts observed with IUE – the IRX- β correlation. The FIR emission results from dust heated by the UV photons it absorbs. Hence, for galaxies obeying this correlation, one can use β to predict the FIR/UV flux ratio, and hence recover the dust-absorbed UV emission. This can be especially useful at high redshift, where access to the rest-frame FIR is currently very difficult. One problem with this method is the heterogeneous nature of the calibrating IUE galaxy sample. It is not yet clear how well this calibration works for FIR-selected (e.g. IRAS) galaxies. We can now begin to address this issue for the most luminous IRAS galaxies.

We have calculated the global values of β and the IRX for our ULIGs (see appendix) after first correcting for Galactic extinction using the values in Table 1. and for the galaxies studied by TKS using the fluxes in that paper. The values for our ULIGs are given in Table 3. We plot β and the IRX in different apertures in Figs. 1 and 2.

The key result is that most of our LIGs and ULIGs do not obey the IRX- β correlation, irrespective of aperture size. The sense of this is that in most cases, our galaxies have much higher IR-excesses for their UV colors than M99’s galaxies. In the absence of the FIR data, using the M99 correlation would lead us to greatly underestimate the FIR fluxes of most of our galaxies. One might have hoped that if the bluer light from star-forming regions far from the nuclei were ignored, the light from the nuclei themselves might follow the IRX- β

correlation, but this is not the case. The discrepancy between our galaxies and the M99 sample gets much worse as we decrease the aperture sizes and split the FIR fluxes between members of interacting pairs (Fig. 2). By far the worse failure is Arp 220, where using the 2 kpc diameter aperture would have us underestimating the FIR flux by a factor of $\sim 10^4$. While the UV colors are indeed redder in the smaller apertures, the UV fluxes themselves drop off as well. On the other hand, VV 114, the second least luminous system in our sample, comes the closest to obeying the IRX- β correlation, falling within the scatter of IUE starbursts. VV 114 is composed of UV-bright and UV-faint components, and it is the former that is similar to M99’s starbursts. (It is possible that the nucleus of IRAS 19254-7245 S is consistent with IRX- β , since we only have a lower limit for β .)

One possible interpretation of the above two results is that the IR-luminous regions of the galaxies are so obscured that we have detected no UV light from them at all. In this case, the UV light we do see comes from relatively lightly-reddened star-forming regions and stars outside the most obscured regions, giving blue colors. We would then expect the IRX to be essentially uncorrelated with color, as is observed. Inspection of Table 3 shows that only on order of a few percent of the total NUV flux arises from the inner 0.5 kpc radius (from 0.07% for VV 114 E to 7.3% for IRAS 15250+3609). This is also consistent with the central, intrinsically luminous regions being hidden from view. This is the expectation of radiative transfer models where stars and dust are mixed, such as the “dusty” model with SMC type dust of Witt & Gordon (2000); see their Fig. 12⁵. However, for a given geometry, the Witt & Gordon models cannot explain both the range of the IRX- β correlation seen in M99’s starbursts (which seems to require foreground dust) and the position of the LIGs and ULIGs (which does not). Either the relative distribution of dust and stars is different between the IUE starbursts and our sample, or a more complicated dust geometry than that explored by Witt & Gordon is required.

This picture has important implications if ULIGs are in fact the analogues of the sub-mm galaxies. We should not expect optical spectroscopy of the sub-mm sources, probing the rest-frame vacuum UV, to be sensitive to the dominant luminosity source in the inner few hundred pc of the galaxies. In some cases, an AGN may be seen through a hole in the obscuring gas and dust; but the absence of an AGN spectrum is not sufficient to rule out the possibility of a buried AGN.

⁵which is mislabeled Fig. 13 in the print version

4.1.2. Optical depths in the ULIGs

Sub-mm line and continuum observations of ULIGs have shown that they contain tremendous concentrations of gas and dust in their nuclei (Scoville et al. 1991; Sanders et al. 1991; Downes & Solomon 1998; Bryant & Scoville 1999). Commonly, $10^{10} M_{\odot}$ of gas are located in the inner kpc of ULIGs. The highest spatial resolution observations show the existence of what Downes & Solomon (1998) called “extreme starburst regions,” wherein $\sim 10^9 M_{\odot}$ of H₂ gas is concentrated in regions typically 100 pc in size. The resulting beam-averaged surface densities of dust (assuming reasonable gas/dust ratios and spherical symmetry) are so high as to give extinctions of up to $10^2 - 10^3$ magnitudes A_V in the inner few hundred pc.

This simple model, which requires $A_K \approx 0.1 A_V \approx 10 - 100$ magnitudes, cannot apply to all parts of the nuclear regions in the ULIGs, since bright near-IR emission is in fact seen from the nuclear regions of all ULIGs (e.g., Scoville et al. 2000). Further, we see UV emission concentrated towards the inner few hundred pc in some of the galaxies, even though the compact nuclear sources are usually not well detected in our images. An alternate picture, as suggested by Downes & Solomon (1998), might be a compact, totally obscured (in the UV, near-IR, and even mid-IR) core (the extreme starburst regions) with still dense, yet not entirely opaque (in the near-IR) mixed gas/dust clouds on the exterior (the surrounding “molecular disk”). On the outside would be additional mixed gas/dust clouds and UV sources, possibly corresponding to “field” star formation. This would allow us to see some relatively blue extended emission and star clusters outside the most obscured regions. If this is true, some of the UV light visible at the apparent IR nuclei would come from foreground stars seen in projection.

4.2. Implications for Lyman-break galaxies

Adelberger & Steidel (2000) suggested that LBGs and ULIGs/sub-mm galaxies are the extreme objects along an increasingly reddened sequence of starbursts. Their paper marks the most detailed attempt yet to unify these apparently disparate objects.

Adelberger & Steidel examined the SEDs of a sample of ULIGs in the mid-IR, FIR, sub-mm, and radio. After computing an “average SED,” they showed that one could predict the bolometric luminosity of a ULIG from observations at any one of those wavelengths, with typical uncertainties of $\sim 0.2\text{--}0.3$ dex.⁶

⁶This relationship is empirical; it can be explained qualitatively by the fact that the dust temperatures,

They then went further, showing that the admittedly few radio and mid-IR observations of $z \sim 1$ galaxies are consistent with the $\text{IRX}-\beta$ relation found for the M99 sample of local starbursts. The existence of IR-luminous galaxies at $z \sim 1$ has been inferred from *Infrared Space Observatory* observations, particularly of the Hubble Deep Field (Aussel et al. 1999). About 16 galaxies with $z \sim 1$ were detected in the $15 \mu\text{m}$ images. At these redshifts, the ISO observations are sensitive to the broad, rest-frame polycyclic aromatic hydrocarbon (PAH) emission features seen in local starbursts. Adelberger & Steidel showed that the FIR luminosity of local ULIGs can be estimated to an accuracy of about 0.22 dex from the strength of these mid-IR features. If that relationship holds at $z \sim 1$, then the ISO-detected galaxies would have FIR luminosities like local ULIGs, but would have lower values of the IRX , approximately following M99’s $\text{IRX}-\beta$ relation. This is some suggestion that while ULIGs exist at $z \sim 1$, they might be different (more transparent) than local ULIGs.

The $\text{IRX}-\beta$ relation might hold at $z > 1$ as well. Rest-frame UV observations of two high- z galaxies, ERO J164502+4626.4 and SMM J14011+0252, are consistent, within errors, with those galaxies obeying the $\text{IRX}-\beta$ relationship. Finally, measurements of the ensemble fluxes (at $850 \mu\text{m}$ and radio wavelengths) of samples of $z \sim 3$ LBGs show that these galaxies are at least not grossly inconsistent with $\text{IRX}-\beta$. The overall conclusion of Adelberger & Steidel is that observations at $z \approx (0, 1, 3)$ are all consistent with the existence of an $\text{IRX}-\beta$ -like relationship holding all the way to high redshifts. In addition, computing the total $L_{\text{tot}} \sim (L_{\text{UV}} + L_{\text{dust}})$, Adelberger & Steidel show that galaxies with higher L_{tot} are more obscured (that is, have a higher value of the IRX) than less bolometrically luminous galaxies. However, it also appears that the slope or zero-point of this relationship evolves with redshift, in that for a given star formation rate, galaxies are more transparent at $z \approx 3$ than at $z \approx 0$.

To further complicate matters, there are some LBGs with fairly high luminosities ($\sim 10^{11} L_{\odot}$) that appear to have very little dust (as determined by the absence of appreciable dust reddening). These objects will have relatively low FIR luminosities if they obey the $\text{IRX}-\beta$ correlation. The LBGs expected to have the highest bolometric luminosities have similar apparent UV magnitudes, but are much redder. They have predicted $L_{\text{bol}} \sim 10^{12} L_{\odot}$ (M99), while the brightest sub-mm galaxies are estimated to be ten times more luminous. Adelberger & Steidel attempted to logically connect these lower-luminosity objects that are detectable in deep optical surveys, to the higher-luminosity dusty objects (sub-mm galaxies are the most extreme examples) that were present in the early universe, yet are not easily detected (if at all) with the same techniques.

calculated from the $60/100 \mu\text{m}$ flux ratios, span only a factor of ~ 2 among ULIGs; the sub-mm observations are in the Rayleigh-Jeans regime; and the radio-FIR correlation has a small dispersion.

As noted earlier, the IRX- β relation at $z \approx 0$ was determined by M99 from observations of a heterogeneous sample of fairly UV-bright starbursts. That sample was not preselected to contain galaxies with high L_{IR} , so it was not clear that LIGs and ULIGs obeyed the IRX- β relationship. The HST observations of three ULIGs by TKS were the first indication that ULIGs in fact deviated from IRX- β . Our new observations confirm that clearly, for the ULIGs in our sample, IRX- β does not hold. The IRX- β relation appears to break down at $\log\left(\frac{F_{FIR}}{F_{FUV}}\right) \sim 2$. Though Adelberger & Steidel (2000) showed that two sub-mm galaxies were consistent with IRX- β , this would not, in general, be the case if our ULIGs are good analogues to sub-mm galaxies.

One point, however, is that not all our galaxies fail IRX- β completely: the LIG VV 114 in particular is not too far off. There are two galaxies in the M99 sample with $L_{IR} \approx 4 \times 10^{11} L_\odot$. One, NGC 3256, obeys IRX- β , while the other, NGC 1614, is overbright in the FIR. It would be interesting to observe more galaxies with $L_{IR} = 10^{11} - 10^{12} L_\odot$ to see if there is some particular value of L_{IR} where galaxies begin to move far off the IRX- β relationship. Our sample is too limited to tell, as it contains only two galaxies in that luminosity range.

We have referred to the breakdown of IRX- β primarily as a luminosity effect, but it may be that dust content and spatial distribution are more important. Dust content and FIR luminosity are correlated, so compared to low-luminosity starbursts, ULIGs have greater amounts of gas and dust available to both fuel and obscure the compact starbursts (or AGN) that provide the high luminosities. Additionally, in ULIGs, this gas and dust is centrally concentrated, usually in the inner kpc or less, resulting in immense optical depths.

4.3. Starbursts vs. AGN

Many of our galaxies evidence strong, nuclear activity not necessarily connected to star formation. Detailed descriptions of each galaxy are given below, but of the galaxies in our sample, Mrk 273 and the southern (IR-dominant) component of IRAS 19254–7245 have Seyfert 2-type optical spectra; the near- and mid-IR properties of VV 114 give evidence that an AGN might be present in the eastern half of the system; and IRAS 08572+3915 NW, IC 883, IRAS 15250+3609, and Arp 220 have LINER spectra. The connection between LINER spectra and AGN activity is still poorly understood; a LINER spectrum might be due to shock-excited gas associated with a starburst-induced “superwind,” and have no relationship to (black hole-inspired) AGN activity at all (Ho 1999; Barth & Shields 2000; Lutz, Veilleux & Genzel 1999).

The best evidence for “dominant” AGN (i.e., producing $\geq 50\%$ of the FIR flux) is

probably in IRAS 08572+3915 NW and IRAS 19254-7245 S. On the other hand, the presence of strong starburst activity (perhaps with a modest AGN contribution) seems well established in the other five galaxies in our sample. This is detailed below in §4.4.

How would the presence of an AGN affect the $\text{IRX}-\beta$ correlation? The starburst fraction of the FIR emission would decrease as the AGN fraction increased. If we detect only the starburst in the UV, and if only the starburst fraction of the FIR emission were counted, this would push the galaxy downward on the $\text{IRX}-\beta$ plots, closer to the relationship found for the UV-selected starburst sample. As noted above, AGN are likely to make a substantial contribution to the FIR in only two cases. VV 114 falls on the $\text{IRX}-\beta$ relationship, the other four likely to be starburst-dominated all fall far above. Thus, a minor AGN contribution to the FIR is not capable of explaining the weak UV detections.

4.4. Individual galaxies

4.4.1. VV 114

VV 114 (IC1623, Arp 236) was discovered to be a bright FIR source in the original IRAS Bright Galaxy Survey. At about 87 Mpc distance, it is one of the more nearby galaxies with such a high FIR luminosity.

Optical and near-IR imaging (Knop et al. 1994; Doyon et al. 1995) show a strong contrast between the two members of the merging pair that comprise VV114. The western component (VV 114 W) is dominated by a blue, high surface brightness complex of regions with a relatively weak near-IR nucleus. The eastern component (VV 114 E) is much redder and brighter in the near-IR, and contains two prominent, extended sources: A and B of Doyon et al. Only the brighter of these, source A, is apparent at $3.8\mu\text{m}$. The HST NICMOS images of Scoville et al. (2000) show that source A contains a bright, pointlike source that had been unresolved in the ground-based images.

Optical and near-IR spectra indicate that star formation dominates the energetics of VV 114 W, while both star formation and an AGN may power VV114E. At $2.2\mu\text{m}$, the latter shows a very red continuum with starburst features (HeI and $\text{Br}\gamma$ nebular emission lines and stellar CO absorption bands) superimposed (Doyon et al. 1995). The near-IR spectrum of region A, can be modelled by a combination of about 50% highly reddened starlight ($A_K \sim 0.5$ mag, for $A_V \sim 5$ mag), and about 50% hot dust ($T \gtrsim 500K$) which is consistent with the broad-band near-IR colors. The high hot dust fraction of the concentrated red emission in source A is very unusual in what otherwise seems to be a starburst (Goldader et al. 1995, 1997a,b). The 5–12 μm colors (from the Infrared Space Observatory, ISO) are

also consistent with strong hot dust emission, leading Laurent et al. (2000a) to suggest that VV 114 E may get up to one-half of its mid-IR luminosity from an AGN. Maps of VV 114 E at 8.44 GHz (Condon et al. 1991) show the multiple morphology seen at 2.2 μm , and the radio counterpart of source A contains several small sources. At lower resolution, radio maps (Condon et al. 1990) show that 21 cm continuum radiation is widespread throughout the system with concentrations corresponding to both VV114W and E. Sub-mm line and continuum maps (Yun, Scoville & Knop 1994; Frayer et al. 1999) show great amounts of molecular gas and dust are present in VV 114, with morphology grossly similar to the 21 cm maps. Much of the material detected in the sub-mm maps is located between VV 114 E and VV 114 W.

The two components of VV114 are probably nearly equal in total luminosity, although their overall SEDs are very different. Using the 21 cm flux as a tracer of FIR, Knop et al. (1994) suggest that the FIR flux is split 60% from E, 40% from W. However, with this split, $F_{\text{FUV}}/F_{\text{FIR}} \sim 0.2$ for the W component, which means that the FUV flux also contributes significantly to the bolometric luminosity. From Starburst99 models (Leitherer et al. 1999) we estimate a bolometric correction of ~ 1.3 for the STIS FUV fluxes of star forming populations⁷, hence the detected FUV emission adds another $\sim 27\%$ to the bolometric flux of the W component. Therefore in terms of bolometric luminosity, the split is about 45% in the E and 55% in the W components.

The contrast between the two components is most extreme in our UV images (Figs. 3-5). These show exquisite detail, and the greatest number of star clusters observed in any of our galaxies. Several hundred clusters are seen in VV 114 W, many visible all the way from the far-UV through near-IR. However, very little UV emission is detected from VV 114 E. No bright UV sources are seen in the near-IR bright regions of VV 114 E. No detectable UV sources are seen projected within ~ 250 pc of B, while two faint, fairly blue UV sources are seen projected about 100 pc from source A. The fairly blue colors of the clusters in VV 114 W, and the similarity of the UV and near-IR images of VV 114 W, suggest that dust absorption is not nearly as strong there as in VV 114 E.

4.4.2. IRAS 08572+3915

IRAS 08572+3915 consists of an obviously interacting, yet still well-separated pair of galaxies. All available data point to the NW component (“IRAS 08572+3915 NW”) as being

⁷This refers specifically to a 100 Myr duration constant star formation rate population having solar metallicity, and a Salpeter IMF with upper mass limit of $100 M_\odot$.

responsible for nearly all of the far-IR luminosity of the pair. It is the only one of the pair detected in mid-IR and radio maps. The other galaxy (“IRAS 08572+3915 SE”) has optical colors similar to quiescent galaxy nuclei and is not detected in VLA maps (Condon et al. 1990) (inspection of those maps shows that the peak surface brightness at the position of SE is $\leq 10\%$ of that at NW) or in the mid-IR, where Soifer et al. 2000 limit the SE source’s contribution to $\lesssim 30\%$ of the total mid-IR flux). Using these non-detections as a guide, we conservatively assign 30% of F_{FIR} to SE (an upper limit, really), and 70% to NW.

There is good evidence that the nucleus of IRAS 08572+3915 NW is very dusty, possibly harboring an AGN. In optical WFPC2 images (Surace et al. 1998), the nucleus is not apparent in the blue ($F439W$) and only begins to show in the I band ($F814W$), while the optical spectrum is that of a LINER (Veilleux, Kim & Sanders 1995). In the near-IR it is extraordinarily red at $2.2 \mu\text{m}$, $f_\lambda \propto \lambda^3$, the reddest of the 56 nuclei studied in the K band spectroscopic study of Goldader et al. (1995, 1997a). In the mid-IR, the morphology is compact, the colors are warm, and the spectrum shows a deep silicate absorption feature (Soifer et al. 2000; Dudley & Wynn-Williams 1997; de Grijp et al. 1985) all of which are indicative of the presence of an AGN.

Our UV images (Figs. 6-8) reveal a morphology quite similar to that seen in the HST $F439W$ images of Surace et al. (1998). Bright emission is seen from the nucleus of IRAS 08572+3915 SE, and HII regions or star clusters are seen in its southern spiral arm; diffuse emission is seen throughout that entire galaxy. Diffuse emission is also seen in the disk of IRAS 08572+3915 NW. However, no peak in the UV emission is seen at the small, red $F814W$ source identified as the nucleus.

4.4.3. IC 883

IC 883 (Arp 193, UGC 8387) shows the appearance of a single, edge-on galaxy, oriented roughly SE-NW. Dust lanes cross through the nuclear region, and reddening may be significant even in the near-IR. A number of objects, probably star clusters, are seen on either side of the disk (Scoville et al. 2000).

Optical spectroscopy (Veilleux, Kim & Sanders 1995) shows IC 883 to have a LINER spectrum. Spectroscopy at $2.2 \mu\text{m}$ (Goldader et al. 1997a) reveals starburst emission lines and stellar CO absorption features. The relatively deep CO index and large Br γ equivalent width argue that the great majority of the continuum at $2.2 \mu\text{m}$ is of stellar origin.

The nuclear region shows two peaks about $0''.75$ apart, embedded in extended emission, at wavelengths ranging from the near-IR, to the mid-IR, and to the radio (Scoville et al.

2000; Soifer et al. 2001; Condon et al. 1991). However, the two peaks do not appear to overlap precisely; their position angles and separations are different in the radio and at 2.2 μm . This might be due to high obscuration even at 2.2 μm or it could be due to multiple sources in the inner $\sim 1.5''$, with great differences in colors. Given the uncertainties in the HST astrometry, we are unable precisely align the radio and HST images, and for the remainder of this paper, we assume that the brightest source at 2.2 μm is coincident with the brightest source at 8.44 GHz. This alignment results a good match of the kpc-scale radio and 2.2 μm light.⁸ Sub-mm observations show an elongated morphology, but do not resolve any pointlike sources (Downes & Solomon 1998).

Our UV images (Figs. 9-10) show faint, patchy extended emission. The extended emission is at a minimum where the near-IR emission is strongest, and there are no prominent UV peaks associated with the nuclear near-IR peaks. There are a few bright pointlike sources in the UV images, probably star clusters, most of which have near-IR counterparts. However, most of the near-IR clusters do not have UV counterparts. We conclude that the extended region in the nucleus, so bright in the near-IR, is quite obscured in the UV. Unfortunately, our STIS images are not optimally centered, and the galaxy probably extends outside our images.

4.4.4. *Markarian 273*

Markarian 273 is a visually striking merging system, with an amorphous central region, a tidal tail stretching ~ 40 kpc nearly due south of the center, and a “tidal loop” counter-tail to the north. Sub-arcsecond resolution imaging from the optical to the radio has revealed three primary sources within the inner 2'' of the galaxy: Mrk 273 N, Mrk 273 SW, and Mrk 273 SE. (Knapen et al. 1997; Soifer et al. 2000; Condon et al. 1991).

Both starburst and AGN activity are found in the central kpc. Mrk 273 has a reddened Seyfert 2 optical emission line spectrum (Veilleux, Kim & Sanders 1999). Yet, a spectrum extending more to the blue (covering 3400-5500Å) presented by González Delgado, Heckman, & Leitherer (2001) is dominated by a reddened stellar continuum with strong Balmer absorption lines. In fact, this new spectrum is well matched by a combination of young, intermediate age, and old stellar populations, though potentially up to $\sim 20\%$ of the optical

⁸Soifer et al. (2001) assumed that the same two peaks are visible in both the radio and IR images, accepting the separation and position angle differences. They noted that their alignment resulted in a poor match between the near-IR and radio kpc-scale emission. While their alignment may well be shown to be correct in the end, it does not substantively affect our conclusions.

light could come from a power-law (AGN?) continuum. While the near-IR spectrum is that of a starburst (Goldader et al. 1995), high-excitation lines signalling an AGN are seen in the mid-IR (Genzel et al. 1998). X-ray observations from the ASCA (Iwasawa 1999) and BeppoSAX (Risaliti et al. 2000) satellites indicated the presence of an obscured, possibly variable, hard X-ray source in the nuclear region. Higher spatial resolution observations from Chandra (Xia et al. 2001) have now revealed a compact, hard X-ray source positionally coincident with Mrk 273 N. Diffuse, softer X-rays are seen from the surrounding nuclear region, and in fact envelop the entire optical structure of the galaxy. No X-ray point sources are found at either Mrk 273 SE or Mrk 273 SW. Unfortunately and importantly, the fraction of L_{bol} produced by the AGN is still not known.

Mrk 273 N is clearly detected as bright, extended region in the near-IR and mid-IR, and some faint optical emission is seen within $0''.1$ of the near-IR peak. Very high-resolution radio observations show that Mrk 273 N is itself bifurcated at the $0''.1$ scale, and may be a rotating disk (Carilli & Taylor 2000). Mrk 273 N appears to be a galactic nucleus—but whether it is the merged nucleus, or the nucleus of only one of the merging galaxies, is not clear.

A strong radio source, Mrk 273 SE is located $0''.75$ from Mrk 273 N. Mrk 273 SE is highly absorbed in HI, suggesting significant optical obscuration, yet at optical and near-IR wavelengths, a blue, rather faint point-like source is visible at the radio position (Scoville et al. 2000). The third major emission region, Mrk 273 SW, shows a bright, point-like peak in near-IR/mid-IR observations, yet its likely radio counterpart is noticeably offset, and weak relative to Mrk 273 N and Mrk 273 SE. Several studies have speculated about the natures of Mrk 273 SE and Mrk 273 SW, and their relationship to Mrk 273 N, but no definitive answers have emerged. Soifer et al. (2000) speculate that consideration of both their spectrophotometric images and the spectroscopy of Dudley (1999) suggests that Mrk 273 N shows silicate absorption at $10 \mu\text{m}$ (indicative of a deeply buried, luminous source, and consistent with the possible X-ray AGN detection), and Mrk 273 SW shows PAH emission (indicative of star formation), but this needs to be confirmed.

Our UV images (Figs. 11-12) show faint, diffuse emission covering an area of $\sim 10'' \times 10''$, with the northern tidal tail being prominent. A few small objects also weakly detected in the WFPC2 image, possibly star clusters, are scattered south of the nuclear region. The most intense UV emission is visible in the vicinity of Mrk 273 N, but is not centered at its radio position. Within the central kpc, the strongest UV emission corresponds with the base of the northern tidal tail, which comes in from the north and apparently terminates ~ 400 pc from the nucleus. No UV peaks are seen at Mrk 273 SE or Mrk 273 SW. No prominent UV emission is spatially coincident with the radio peaks of any of the three principal sources,

though perhaps some is *associated* with these sources. No direct detection of an AGN is made in the UV. While it is possible that some of the UV emission in the nuclear region might be reflected or scattered light from the AGN, the extended UV light seems most likely due to star formation, reinforcing the conclusions of González Delgado, Heckman, & Leitherer (2001).

4.4.5. *IRAS 15250+3609*

IRAS 15250+3609 is one of the original 10 IRAS ULIGs (Sanders et al. 1988). However, for reasons that are not clear, it has been poorly studied. On large scales, the WFPC2 images show a tidal tail visible in earlier ground-based images, as well as several other galaxies of mixed morphological type; we speculate that perhaps they form a group with IRAS 15250+3609. The central region is complex, with several star clusters and extended emission scattered over an area about 4'' in diameter. The WFPC2 images, however, show that the brightest near-IR source is only partly visible in the optical image, apparently obscured by a dust lane.

IRAS 15250+3609 has a LINER-like optical spectrum and a fairly typical starburst near-IR spectrum (Veilleux, Kim & Sanders 1995; Goldader et al. 1997a). ISO spectroscopy reveals strong PAH emission at 7.7 μm , suggesting that star formation plays a prominent role in this galaxy (Genzel et al. 1998). However, the upper limits on the high-excitation mid-IR lines are not good enough to rule out the presence of an AGN. The center of IRAS 15250+3609 contains a compact, yet resolved ($\theta \sim 0''.2$) radio source (Smith et al. 1998), consistent with a concentrated region of star formation. The available evidence points towards star formation dominating the energetics of IRAS 15250+3609.

Our STIS images (Figs. 13-14) show that the UV morphology of the central region is similar to the optical morphology. Most of the optically visible clusters are UV-bright. While some faint, extended emission is present throughout much of the nuclear region, no bright UV source is seen at the location of the brightest near-IR source.

4.4.6. *Arp 220*

Though Arp 220 has often been called “the prototypical ultraluminous infrared galaxy,” progress towards understanding this, the nearest ULIG, has occurred slowly, and with many about-turns.

Arp 220 has a highly complex optical morphology, with light extending over at least 40

kpc. In the midst of an optically dark dust lane, IR and radio images revealed two prominent emission regions about $1''$ (370 pc) apart (Graham et al. 1990; Condon et al. 1991). These mark what may be the nuclei of the merging galaxies. VLBI imaging has shown the radio-emitting regions to contain numerous milliarcsec-scale sources, which have been interpreted as radio-luminous supernova remnants (Smith et al. 1998).

Optical spectroscopy of Arp 220's nuclear region has revealed a LINER spectrum, and strong superwind activity is present (Kim, Veilleux & Sanders 1998; Heckman, Armus & Miley 1987). Spectroscopy of the two near-IR peaks reveals very strong stellar CO absorption features in the K -band, proving that starlight dominates the continuum at $2.2\mu\text{m}$, and there is no evidence of broad emission lines (Goldader et al. 1995). ISO mid-IR and FIR spectroscopy also reveals only starburst features (Genzel et al. 1998 and references therein).

Downes & Solomon (1998) presented a detailed argument showing that there is sufficient detected starburst activity to power Arp 220, and thereby excluding the presence of a powerful AGN. It is probably fair to say that there is no direct evidence, at this time, in favor of a luminous AGN in Arp 220.

Our UV images (Figs. 15-16) reveal that the central kpc of Arp 220 emits no concentrated UV light. However, extremely faint extended emission is present over nearly the entire STIS field of view, and the darkest areas of our images are located within the dust lanes so prominent in optical images. A small number (~ 3) of the star clusters visible in the $F814W$ image have clear UV counterparts, and a small extended patch visible just east of center in the UV images has a very weak counterpart in the $F814W$ image.

4.4.7. *IRAS 19254-7245*

IRAS 19254-7245 is best known as the “Superantennae” (Mirabel, Lutz & Maza 1991). With tidal tails 350 kpc across, it is a merger in progress. Despite the similar optical appearances of the two galaxies, ISO observations (Laurent et al. 2000a,b) indicate that a Seyfert 2 nucleus (Mirabel, Lutz & Maza 1991) in the southern galaxy produces at least 70% of the mid-IR luminosity and perhaps almost all the FIR luminosity.

The $F814W$ images show that both nuclei are extended, with complex morphologies at even $0''.1$ scales. We identify the bright $F814W$ source in the southern nucleus as the AGN, since the optical spectrum is dominated by AGN features. Our STIS images (Figs. 17-18) show very weak and diffuse FUV and NUV emission from the spiral arms, plus a few faint star clusters. Only in the NUV image is concentrated emission seen near the optical nuclei. There is an elongated NUV source coincident with the southern nucleus $F814W$

peak, making this galaxy the only one of our sample where a reasonably prominent UV source is clearly detected at the supposed IR peak. Though readily apparent, however, the source is not very bright. In the 0.5 kpc radius aperture, the southern nucleus is almost 2.2 magnitudes fainter in the NUV than IRAS 15250+3609, and more than 1.7 magnitudes fainter than IRAS 08572+3915 SE (corrected for Milky Way extinction), both at comparable distances. Further, since the NUV structure of the southern nucleus is clearly extended, we suggest that it may trace an edge-on circumnuclear disk, a jet, or even a star-forming region, rather than the AGN itself.

5. Discussion

5.1. Detecting ULIGs in the UV

Including the three ULIGs from TKS, all ULIGs observed in the vacuum UV by HST have been detected. These galaxies often show both extended emission from unresolved stars, and luminous star clusters. In our sample, the UV emission tends to be (5/7 cases) strongest projected against the inner kpc, yet even then it is often faint and there are two cases (VV 114 E and Arp 220) where very little emission comes from the inner kpc. However, in 6 of 7 galaxies, there are significant offsets, several hundred pc or more, between the UV peaks and near-IR peaks. If the near-IR and radio morphologies of the galaxies in our sample accurately represent the morphologies of the dominant FIR energy sources, then our UV images do not, in general, pinpoint the locations of principal energy generation.

5.2. Detecting ULIGs at high redshift

An important part of our study is to determine how these ULIGs would appear at high redshifts, in deep surveys such as the Hubble Deep Field.

For a galaxy with rest-frame monochromatic luminosity L_ν , observed at some high redshift with luminosity distance d_L , the observed monochromatic flux density f_ν is $f_\nu = \frac{L_\nu \times (1+z)}{4\pi d_L^2}$. The flux density at some high redshift z_{high} , in terms of the flux density observed at the true redshift z_{true} is then:

$$f_{\nu, z_{\text{high}}} = f_{\nu, z_{\text{true}}} \times \frac{d_{L, z_{\text{true}}}^2 (1 + z_{\text{high}})}{d_{L, z_{\text{high}}}^2 (1 + z_{\text{true}})}. \quad (1)$$

We neglect the fact that, since our ULIGs are at an average redshift of $z = 0.046$, we are observing light emitted at slightly shorter wavelengths than the pivot wavelengths of our UV

filters.

The light seen from each galaxy in the NUV filter would be redshifted into the $F606W$ filter ($\lambda_{\text{pivot}} = 6002\text{\AA}$) at $z = 1.54$. The light seen from each galaxy in the FUV filter would be redshifted into the $F606W$ filter at $z = 3.12$. We computed the high redshift fluxes after correcting the data for Milky Way UV foreground extinction. We have predicted the surface brightnesses (in AB magnitudes arcsec^{-2}) of the light within the half-light radii (Fig. 19) for each component of our sample galaxies. These are given in Table 4. For the single galaxies, an aperture radius of 5 kpc includes $\geq 85\%$ of “total” flux (see columns 6 and 7 of Table 3; aperture growth curves are given in Fig. 19). We therefore define the half-light radius as that containing half of the light in the 5 kpc radius aperture.⁹

Though the total fluxes of at least some of the galaxies are within reach of, e.g., the HDF, the surface brightnesses are strongly affected by the cosmological surface brightness dimming. The HDF limiting magnitudes in $F606W_{AB}$ is 28.21 (10σ) for point sources (Williams et al. 1996). However, Totani & Yoshi (2000) show that no galaxies were detected in the HDF with average surface brightnesses less than 27.5 AB mag arcsec^{-2} in $F606W$. We worked out the surface brightnesses of our galaxies, using the radii containing half the light in the 5 kpc physical apertures (Table 4).

We also used the data tables of the HDF galaxies (Williams et al. 1996) to compute the surface brightnesses at $F606W$, assuming that r_1 , the “first moment radius,” is equivalent to the half-light radius (Fig. 20). We would expect to detect all galaxies except Arp 220 in $F606W$ at $z = 1.54$, but only VV 114 W and IR 15250+3609 would be above the detection threshold by $z = 3.12$. Perhaps the next brightest couple could be seen at the few σ level. If the surface brightness detection limit can be pushed a magnitude deeper, then all our sources would be detectable out to $z = 1.5$ and about half would be, if placed at $z = 3.1$.

5.3. ULIGs and Lyman break galaxies

A major part of our study was to determine how the properties of our ULIGs, if placed at $z \sim 3$, would compare with those of the Lyman break galaxies discovered at similar redshifts.

To this end we compare our ULIGs to the 100 Hubble Deep Field U-band dropouts

⁹This definition of the half-light radius fails for VV 114 E, where photometry in the 5 kpc radius aperture is dominated by flux spilling over from VV 114 W. We therefore ignore VV 114 E for the high-redshift discussions.

studied by M99 in Fig. 21. This shows our $z = 3.12$ predictions of V_{606} vs. measured β for the ULIGs compared to the observed V_{606} vs. $V_{606} - I_{814}$ color of the U -dropouts. The $V_{606} - I_{814}$ color is scaled to β using equation 12 of M99. The dotted line shows the selection limits for U -dropouts used by M99. This figure is analogous to the top panel of Fig. 5 of M99, without the absorption correction and without correcting to absolute magnitude (we do present the absolute FUV magnitudes of our galaxies, corrected for foreground and also for internal absorption, in Table 5).

We find that most ULIGs would be too faint to have been selected as U -dropouts by M99. The flux limits used by M99 were adopted to conform to those used by Madau et al. (1996). While Fig. 20 shows that if ULIGs were placed at these redshifts, many would have magnitudes within the cloud of observed HDF *detections*, their fluxes are so weak that they would not make it into reputable catalogs of reputable U -dropouts. Typically the selection limits (and hence detection limits) would have to be pushed 2 magnitudes deeper at $z \sim 3$ to find exact analogs of our ULIGs if they exist. In addition to being too faint, three of the ULIGs would be too red to be selected as U -dropouts.

The key result is that, if placed at $z \sim 3$, only 1 of 7 galaxies in our sample would appear as a U -band dropout in the HDF. The galaxy VV 114 has the UV color, luminosity, and size typical of LBGs, and hence makes a good local analog. But while the UV light may recover half of the bolometric luminosity after reddening corrections, it still avoids the dominant source in the near-IR. Our data show that ULIGs do not overlap with the brighter Lyman break galaxies. In most ULIGs, the galaxies are so UV-faint and UV-extinguished that they could never be selected as LBGs in the first place.

5.4. ULIGs and Extremely Red Objects

It has recently been determined that some sub-mm galaxies are Extremely Red Objects (EROs: $R - K \gtrsim 6$ in the Johnson-Cousins system; Dey et al. 1999, Smail et al. 1999, Frayer et al. 2000). Would our galaxies be EROs?

We predicted the R -band fluxes of our galaxies at $z = 1.96$ (where the NUV filter would sample the rest-frame R band) and at $z = 3.80$ (where the FUV filter would go to R) as outlined in §5.2, converting them from AB magnitudes to the Johnson-Cousins system in this case.

We estimated the observed K -band fluxes of our galaxies at $z = 1.96$ and $z = 3.80$ using optical photometry from the literature, in a manner similar to our calculations above. We restricted our optical photometry to two papers, for the sake of uniformity. Mirabel, Lutz

& Maza (1991) obtained photometry of the two components of IRAS 19254–7245 through standard *BVRI* filters in an 8" diameter aperture, nearly matching our 5 kpc radius aperture (4".245 radius). For IRAS 08572+3915 NW, Mrk 273, IR 15250+3609, and Arp 220, we used *Bgri* photometry from Sanders et al. (1988) in 10" diameter apertures, which match fairly well the dimension of the 5 kpc radius apertures given in Table 3. We converted the *gri* photometry to the Johnson system using the transformations given by Thuan & Gunn (1976) and Wade et al. (1979). Our predicted values for R , K , and $R - K$ are given in Table 6.

Of the IR-dominant nuclei in Table 6, 4 of 5 would have $R - K > 4$, 3 of 5 would have $R - K > 5$, and 1 of 5 would have $R - K > 6$, for at least one of the two redshifts. We note that Arp 220 has $R - K = 5.95$ at $z = 3.80$, and so within reasonable uncertainties, might appear as an ERO if at that redshift, giving us 2 out of 5 of our ULIGs that might be selected as EROs at an appropriate redshift in the range $1.96 \leq z \leq 3.80$.¹⁰

5.5. ULIGs and Sub-mm galaxies

ULIGs are the only objects in the local universe ($z < 0.1$) with thermal FIR emission even approaching that of the sub-mm galaxies. This makes ULIGs the most likely local counterparts of sub-mm galaxies—but is there a direct match? In other words, are ULIGs the local (low- L , low- z) tail of the same class of objects we see as sub-mm galaxies at $z > 1$? Or are local ULIGs and sub-mm galaxies different kinds of objects, which both happen to have high FIR luminosities?

First, we return to the fact that the current sample of sub-mm galaxies are intrinsically a few times more luminous than any local ULIG. Even the most luminous of our ULIGs, Arp 220, would have an observed 850 μm flux $\lesssim 2$ mJy at $z = 1 - 3$, and so it would not be present in the current lists of 3σ or 4σ SCUBA sources. The uncomfortable conclusion is that our ULIGs, if placed at $z > 1$, would be difficult or impossible to detect in either optical or sub-mm deep fields.

One argument that local ULIGs are not like those at high redshift can be drawn from the work of Adelberger & Steidel (2000) discussed earlier. At $z > 1$, IR-luminous galaxies appear to be more transparent in the UV than local ULIGs. The reasons for this are not

¹⁰However, the “success” rate depends strongly on how one defines it; we might say that 5 galaxies at 2 redshifts gives 10 cases, with only 10% clearly resulting in an ERO. Our main goal is to determine if *any* of our galaxies might be selected as an ERO in the redshift range appropriate to sub-mm galaxies and LBGs, and the answer appears to be “yes.”

obvious. One possibility, shown directly in the sub-mm galaxy SMM J14011+0252 galaxy (and hinted at in others) by Ivison et al. (2001), is that the IR-emitting regions in sub-mm galaxies are much more extended than in local ULIGs. This would naturally lead to a greater chance for “holes” in the obscuration from which UV light could escape.

One way to see if ULIGs and sub-mm galaxies are the same kinds of object is to ask the question: do the rest-frame UV/optical properties of our ULIGs match those of the sub-mm galaxies?

Ivison et al. (2000) divide the observed sub-mm counterparts into three classes. Class II galaxies are bright, with obvious optical counterparts. Class I galaxies are bright at K , but faint in optical: they are bright EROs. Class 0 galaxies have no obvious counterparts down to $I \sim 26$, $K \sim 21$. Frayer et al. (2000) examine nine sub-mm sources, and suggest that 40%–70% of the sub-mm population are in very faint or red galaxies; two of these ($\sim 20\%$) are EROs (Class I). Our ULIGs and LIGs exhibit a wide range of rest-frame UV/optical properties, reminiscent of the sub-mm galaxies. We found that some of our ULIGs might appear as EROs at either $z = 1.96$ or $z = 3.80$. But the sub-mm EROs are bright at K , and at those redshifts, our ULIGs would be faint. Only one of the five ULIGs in our sample (IRAS 08572+3915) would have $K < 21$ at $z = 1.96$; by $z = 3.80$, all would have $K > 23$. Even scaling up the UV fluxes from our ULIGs by factors of a few (to match the FIR luminosity differences) would not be sufficient to render them easily observable. In summary, our ULIGs (at $z = 1.96$ and $z = 3.80$) would all be fainter and redder than the Class II sources; mostly fainter than the Class I sources; and so might only be true counterparts of the Class 0 sources.

Where are the local Class II and Class I counterparts? We speculate on three possibilities. First, the number of ULIGs increases strongly with redshift, so perhaps Class I/II galaxies are simply vanishingly rare at low redshift. Second, perhaps differences in properties such as metallicity result in the sub-mm galaxies being more transparent in the rest-frame UV/optical than the ULIGs. Third, while local ULIGs occur almost exclusively in recent or ongoing mergers, perhaps sub-mm galaxies are made in a different way, with corresponding differences in properties. The extended nature of SMM J14011+0252 hints at this tantalizing possibility. In the local universe, generating $> 10^{12} L_\odot$ in a galaxy appears to virtually always require a collision and subsequent collapse of the ISM to a dense state in the inner kpc. Perhaps galaxies were somehow able to generate these energies without such collapse at high redshifts. If this is true, then local ULIGs would likely not be good counterparts of sub-mm galaxies. Any real study of the differences awaits much more data on sub-mm galaxies.

5.6. VV 114, IRAS 08572+3915, and SMM J14011+0252 J1/J2

In two of our systems, VV 114 and IRAS 08572+3915, we have merging galaxies where one member of each pair is bright in the UV, but the other is much brighter in the near-IR and mid-IR, and (possibly, for VV 114) the FIR as well. If these two systems were sub-mm sources at high redshifts, then optical observations, sensitive to the rest-frame UV, might not even detect the less UV-luminous—and more IR-luminous—member of each pair. The member of the pair responsible for most of the FIR luminosity would become apparent only in mid-IR observations, which are difficult to perform from the ground. On the other hand, optimistically speaking, we might say that we have *two* chances to detect early-stage merging systems.

Ivison et al. (2000) and Smail et al. (2000) describe the sub-mm selected galaxy SMM J14011+0252 ($z = 2.55$), which may be a high redshift example of this. That system contains two principal components, the morphologically complex J1, and the relatively compact J2. J2 is slightly brighter than J1 at rest-frame UV wavelength of 1000Å (observed *U*-band), whereas J1 is brighter than J2 longward of the Lyman break (observed *B*-band, $\lambda_{rest} \approx 1240\text{\AA}$) and in the rest-frame red optical (observed *K*-band, $\lambda_{rest} \approx 6200\text{\AA}$). From the above, we know that J1 would be stronger than J2 at the rest-frame wavelengths of both our FUV and NUV observations.

Very recently, Ivison et al. (2001) showed that SMM J14011+0252 is significantly extended in both interferometric CO and radio maps ($\gtrsim 10$ kpc in the source plane). Further, the CO/radio peaks are apparently coincident, but not located at either J1 or J2. Instead, the CO/radio peak seems to be associated with a newly-discovered, diffuse ERO component (J1n), about an arc-second north of J1. This is reminiscent again of VV 114, where the CO and sub-mm emission both peak away from the prominent UV/optical/near-IR sources Frayer et al. (1999).

Adelberger & Steidel (2000) note that SMM J14011+0252 is globally consistent with the $\text{IRX}-\beta$ correlation, though the rest-frame UV flux is the sum from J1 and J2. (Likewise, VV 114 is *globally* consistent within the scatter of $\text{IRX}-\beta$.) Our observations—via analogy to VV 114 and IRAS 08572+3915—also suggest that J2 need not dominate the FIR emission from the entire source. That the radio peak is apparently associated with a newly-discovered, extended ERO region further suggests this. Our study shows that while rest-frame UV images may be useful to detect merging galaxies, they do a rather poor job of pinpointing the dominant energy sources, which may be inconspicuous at rest-frame UV wavelengths.

6. Conclusions

We have presented new UV images of a sample of seven LIGs and ULIGs taken with the HST. Our principal results are as follows.

1. All seven of our ULIGs were detected in the UV. They show star clusters and extended emission, with the brightest UV light projected within the central kpc of the most IR-luminous members of the systems in 5/7 cases.
2. However, the UV peaks are displaced by at least few hundred pc from the peaks in *I*-band and near-IR images, and so presumably the far-IR peaks as well. At most a few percent of the total UV light comes from the inner 500 pc, where the majority of the far-IR energy is generated.
3. Most nuclei are reddened. However, even after correction for dust reddening using the $\text{IRX-}\beta$ correlation, the observed light even in large apertures is insufficient, by factors of 3–75, to account for the far-IR emission. When the UV light in 2 kpc diameter apertures is compared with the FIR emission, the deficits typically range from 2–4 orders of magnitude; hence, the reddening is insufficient to account for the large infrared-excesses. We conclude that the compact nuclear starbursts or AGN that dominate the bolometric energies of these galaxies are highly obscured in the UV.
4. All of the galaxies in this study have been previously noted as showing signs of some AGN activity, usually via Seyfert 2 or LINER spectra. However, AGN are not clearly the source of the high infrared excesses in most cases. In only two cases, IRAS 08572+3915 NW and IRAS 19254–7245 S, is it likely that AGN could dominate the bolometric energy output of the system; the majority appear to be dominated by star formation. In only one of the two possible AGN, IRAS 19254–7245 S, we may detect direct UV emission from the AGN. Even in this case, there is no emission in the FUV, and the NUV source is extended, suggesting that a circumnuclear disk, jet, or even star formation may be what is seen in the NUV.
5. Artificially redshifting the UV fluxes shows that six of our galaxies would be detectable in HDF-type exposures out to redshifts of at least $z = 1.54$, yet cosmological surface brightness dimming would render all but two undetectable by $z = 3.12$. The galaxies would also have sub-mm fluxes below current detection limits, if placed in that redshift range. Current optical and sub-mm surveys would therefore probably not detect most of our ULIGs, some of the most luminous objects in the local universe, if they were placed at redshifts much greater than 1.5.

6. We have compared our galaxies with 100 U -band dropouts at $z \approx 3$ from the HDF. If placed at $z \sim 3$, most of our galaxies would be 2–3 magnitudes too faint for robust selection as U -band dropouts in catalogs with HDF-like depths. Only one of our galaxies, the UV-bright member of VV 114, would have made it into the HDF sample. This suggests that ULIGs will not be found in samples of bright Lyman-break galaxies, though some could perhaps be lurking amongst the fainter and redder LBGs.
7. From estimating the R and K -band fluxes at $z = 1.96$ and $z = 3.80$ for the IR-dominant nuclei of our five ULIGs, we find that 2/5 of them would have colors very close to those of Extremely Red Objects. While some ULIGs may appear as EROs at high- z , in general, their faint but significant UV emission makes them somewhat too blue to be classified as EROs.
8. While our sample is small, the predicted faintnesses and red colors of our ULIGs, if placed at high redshift, are reminiscent of the extremely faint/red counterparts of many sub-mm galaxies. However, many sub-mm galaxies have counterparts brighter and/or bluer than our ULIGs would be at $z \approx 2$ or $z \approx 3.8$. One sub-mm galaxy has been shown to have an extended radio source; if this is generally true, then that would call into question the use of ULIGs as low-redshift counterparts.

We thank Neil Trentham for many fruitful discussions concerning cosmology and his earlier papers, and for reviewing drafts of this paper. Nick Scoville kindly provided the adaptive smoothing algorithm we used, and made his team’s NICMOS data available to the community in reduced form. We thank the anonymous referee for insightful comments and suggestions. Support for Proposal number GO-08201 was provided by NASA through a grant from the Space Telescope Science Institute, which is operated by the Association of Universities for Research in Astronomy, Incorporated, under NASA contract NAS5-26555. This research has made use of the NASA/IPAC Extragalactic Database (NED) which is operated by the Jet Propulsion Laboratory, California Institute of Technology, under contract with the National Aeronautics and Space Administration.

A. Modeling HST/STIS Fluxes

The modeling of HST/STIS fluxes was necessary in order to correct the Galactic foreground extinction within the broad NUV and FUV bandpasses ($\Delta\lambda/\lambda = 0.38, 0.17$ respectively) and to calibrate the relationship between the STIS photometric UV color and the

UV spectral slope β ($f_\lambda \propto \lambda^\beta$). We employed observed spectra and continuous and instantaneous star formation synthetic spectra obtained from the Starburst99 library (Leitherer et al. 1999) for a Salpeter IMF slope $\alpha = 2.35$ with an upper mass limit of $100 M_\odot$, metallicities of $Z = 0.04, 0.02$ and 0.004 , and 21 burst ages ranging from 1 to 900 Myr. Fluxes in broad band filters were measured from the modelled and observed spectra.

A.1. Galactic Extinction

We examined the effect of Galactic extinction on the above model spectra after also applying intrinsic reddening. This was modelled with the Calzetti (1997) mean starburst attenuation curve for $0 \leq E(B - V)_{stars} \leq 1$ with increments of $\Delta E(B - V)_{stars} = 0.1$. Each was redshifted to $z = 0.04$ – typical of our FIR galaxy sample. Finally, the redshifted starburst spectra were reddened for Galactic foreground using the Galactic extinction curve of Cardelli, Clayton & Mathis (1989) for $0 \leq E(B - V)_{Gal} \leq 1$ with increments of $\Delta E(B - V)_{Gal} = 0.05$. Thus, 220 combinations of intrinsic and Galactic reddening were applied to each burst age (21) and metallicity (3) resulting in 13,860 model spectra.

The observed UV color is a function of an unknown intrinsic UV color and a reasonably well known Galactic reddening. The relationship between the UV color excess $E(FUV - NUV)$ and the Galactic extinction parameter $E(B - V)_{Gal}$ was modeled as a quadratic function of the form.

$$E(FUV - NUV) = a E(B - V)_{Gal} + b E(B - V)_{Gal}^2 \quad (A1)$$

where a and b are linear functions of the observed UV color. The same was done for the relationship between the FUV extinction (A_{FUV}) and $E(B - V)_{Gal}$. A range of solutions for the coefficients a and b were determined by a least squares polynomial fit for each curve of constant intrinsic reddening and burst age in the $E(FUV - NUV)$ - $E(B - V)_{Gal}$ or A_{FUV} - $E(B - V)_{Gal}$ plane. A linear fit was then performed for each coefficient as a function of observed UV color; giving the final solutions of:

$$\begin{aligned} a_{E(FUV-NUV)} &= 0.78 + 0.155 (FUV - NUV) \\ b_{E(FUV-NUV)} &= 0.559 \\ a_{A_{FUV}} &= 8.749 - 0.077 (FUV - NUV) \\ b_{A_{FUV}} &= 0.141 + 0.007 (FUV - NUV), \end{aligned}$$

where $(FUV - NUV)$ is the UV color measured from the model spectra in AB magnitudes. The technique correctly determines A_{FUV} to within ± 0.03 magnitudes and $E(FUV - NUV)$

to within ± 0.05 magnitudes provided that $E(B - V)_{Gal} \leq 0.4$. The fit improves with decreasing $E(B - V)_{Gal}$. A fit to A_{NUV} was not as successful due to the large width of the NUV bandpass. This method also fails for older stellar populations, such as post-instantaneous burst with ages > 300 Myr. The net effect of this correction on our sample is small. The average A_{FUV} increases by 0.01 magnitudes and $E(FUV - NUV)$ increases by 0.03 magnitudes.

A.2. Calibrating STIS UV color and β

We use the UV spectral slope β defined by Calzetti, Kinney & Storchi-Bergmann (1994) within 10 narrow windows between 1268 and 2580 Å. These windows avoid many of the emission and absorption features in the UV. IUE spectral data for 33 starburst galaxies (Kinney et al. 1993) were used in addition to 693 synthetic starburst spectra. The metallicity and age parameters of the synthetic starburst spectra were described previously; however, only models with continuous star formation rates were used.

The IUE data were redshifted to $z = 0.04$ with no further processing. Intrinsic reddening was applied to the restframe starburst spectra in accordance with the Calzetti, Kinney & Storchi-Bergmann (1994) mean starburst attenuation curve for $0 \leq E(B - V)_{stars} \leq 1$ and then redshifted to $z = 0.04$.

The broad band UV color ($FUV - NUV$) was measured directly from these spectra and fit to β as defined above (and measured in the rest-frame). Comparing the UV color to β reveals the robust linear relationship:

$$\beta = -2.20 + 1.88(FUV - NUV), \quad (A2)$$

determined from a minimized chi-square fit. Here, FUV and NUV are measured in AB magnitudes. The fit is secure, with an rms scatter of 0.04 in β , over the range of STIS UV colors modeled ($-1.5 < (FUV - NUV) < 1.5$).

REFERENCES

- Adelberger, K. L., & Steidel, C. C. 2000, ApJ, 544, 218
 Aussel, H., Cesarsky, C. J., Elbaz, D. & Starck, J. L. 1999, A&A, 342, 313
 Barger, A. J., Cowie, L. L., Smail, I., Ivison, R. J., Blain, A. W., & Kneib, J.-P. 1999a, ApJ, 117, 2656

- Barger, A. J., Cowie, L. L., & Sanders, D. B. 1999, ApJ, 518, L5
- Barth, A. J., & Shields, J. C. 2000, PASP, 112, 753
- Bryant, P. M., & Scoville, N. Z. 1999, AJ, 117, 2632
- Calzetti, D., Kinney, A. L., & Storchi-Bergmann, T. 1994, ApJ, 429, 582
- Cardelli, J. A., Clayton, G. C. & Mathis, J. S. 1989, ApJ, 345, 245
- Carilli, C. L., & Taylor, G. B. 2000, ApJ, 532, L95
- Carroll, S. M., & Press, W. H., & Turner, E. L. 1992, ARA&A, 30, 499
- Chapman, S. C. et al. 2000, MNRAS, 319, 318
- Condon, J. J., Helou, G., Sanders, D. B., & Soifer, B. T. 1990, ApJS, 73, 359
- Condon, J. J., Huang, Z.-P., Yin, Q. F., & Thuan, T. X. 1991, ApJ, 378, 65
- de Grijs, M. H. K., Lub, J., & de Jong, T. 1985, Nature, 314, 240
- Dey, A. et al. (1999), ApJ, 519, 610
- Downes, D., & Solomon, P. M. 1998, ApJ, 507, 615
- Doyon, R., Nadeau, D., Joseph, R. D., Goldader, J. D., Sanders, D. B., & Rowlands, N. 1995, ApJ, 450, 111
- Dudley, C. C. 1999, MNRAS, 307, 553
- Dudley, C. C. & Wynn-Williams, C. G. 1997, ApJ, 488, 720
- Frayer, D. T., Ivison, R. J., Smail, I., Yun, M. S., & Armus, L. 1999, ApJ, 118, 139
- Frayer, D. T., Smail, I., Ivison, R. J., & Scoville, N. Z. 2000, AJ, 120, 1668
- Genzel, R. et al. 1998, ApJ, 498, 579
- Goldader, J. D., Joseph, R. D., Doyon, R., & Sanders, D. B. 1995, ApJ, 444, 97
- Goldader, J. D., Joseph, R. D., Doyon, R., & Sanders, D. B. 1997a, ApJS, 108, 449
- Goldader, J. D., Goldader, D. L., Joseph, R. D., Doyon, R., & Sanders, D. B. 1997b, AJ, 113, 1569
- González Delgado, R. M., Heckman, T. M., & Leitherer, C. 2001, ApJ, 546, 845

- Graham, J. R., Carico, D. P., Matthews, K., Neugebauer, G., Soifer, B. T., & Wilson, T. D. 1990, ApJ, 354, L5
- Hauser, M. et al. 1998, ApJ, 508, 25
- Heckman, T. M., Armus, L., & Miley, G. K. 1987, AJ, 92, 276
- Heckman, T. M., Robert, C., Leitherer, C., Garnett, D. R & vsd der Rydt,, F. 1998, ApJ, 503, 646
- Helou, G., Khan, I. R., Malek, L., & Boehmer, L. 1988, ApJS, 68, 151
- Ho, L. C. 1999, Advances in Space Research, 23, 813
- Holland, W. S., et al. 1999, MNRAS303, 659
- Ivison, R. J., et al. 1998, MNRAS, 298, 583
- Ivison, R. J., et al. 2000, ApJ, 542, 27 (2000a)
- Ivison, R. J., et al. 2000, MNRAS, 315, 209 (2000b)
- Ivison, R., Smail, I., Frayer, D., Kneib, J.-P. & Blain, A. 2001, ApJ, in press (astro-ph/0110085)
- Iwasawa, K. 1999, MNRAS, 302, 96
- Kim, D.-C., Veilleux, S. & Sanders, D. B. 1998, ApJ, 508, 627
- Kinney, A. L., Bohlin, R. C., Calzetti, D., Panagia, N. & Wyse, R. F. G. 1993, ApJS, 86, 5
- Knapen, J. H. et al. 1997, ApJ, 490, L29
- Knop, R. A., Soifer, B. T., Graham, J. R., Matthews, K., Sanders, D. B., & Scoville, N. Z. 1994, AJ, 107, 920
- Laurent, O., et al. 2000a, A&A, 359, 887
- Laurent, O., et al. 2000b, A&A, in preparation
- Leitherer, C., et al. 1999, ApJS, 123, 3
- Lutz, D., Veilleux, S., & Genzel, R. 1999, ApJ, 517, L13
- Madau, P., Ferguson, H. C., Dickinson, M. E., Giavalisco, M., Steidel, C. C. & Fruchter, A. 1996, MNRAS, 283, 1388

- Meurer, G. R., Heckman, T. M., Leitherer, C., Kinney, A., Robert, C., & Garnett, D. R. 1995, AJ, 110, 2665
- Meurer, G. R., Heckman, T. M., Lehnert, M. D., Leitherer, C., & Lowenthal, J. 1997, AJ, 114, 54
- Meurer, G. R., Heckman, T. M., & Calzetti, D. 1999, ApJ, 521, 64 (M99)
- Mirabel, I. F., Lutz, D., & Maza, J. 1991, A&A, 243, 367
- Risaliti, G., Gilli, R., Maiolino, R., & Salvati, M. 2000, A&A, 357, 13
- Sanders, D. B. et al. 1988, ApJ, 325, 74
- Sanders, D. B., Scoville, N. Z., & Soifer, B. T. 1991, ApJ, 370, 158
- Sanders, D. B., Egami, E., Lipari, S., Mirabel, I. F., & Soifer, B. T. 1995, AJ, 110, 1993
- Sanders, D. B., & Mirabel, I. F. 1996, ARA&A, 34, 749
- Scoville, N. Z., Sargent, A. I., Sanders, D. B., & Soifer, B. T. 1991, ApJ, 366, 5
- Scoville, N. Z., et al. 2000, AJ, 119, 991
- Smail, I., et al. 1999, MNRAS, 308, 1061
- Smail, I., Ivison, R., Blain, A., & Kneib, J.-P. 2000, to appear in proceedings of U. Massachusetts/INAOE Conference “Deep Millimeter Surveys”
- Smith, H. E., Lonsdale, C. J., & Lonsdale, C. J. 1998, ApJ, 492, 137
- Soifer, B. T., et al. 1987, ApJ, 320, 238
- Soifer, B. T., Boehmer, L., Neugebauer, G., & Sanders, D. B. 1989, AJ, 98, 766
- Soifer, B. T., et al. 2000, AJ, 119, 509
- Soifer, B. T., et al. 2001, AJ, in press (astro-ph/0106172)
- Surace, J. A., Sanders, D. B., Vacca, W. D., Veilleux, S., & Mazzarella, J. M. 1998, ApJ, 492, 116
- Surace, J. A., & Sanders, D. B. 2000, AJ, 120, 604
- Thuan, T. X., & Gunn, J. E. 1976, PASP, 88, 543

- Totani, T., & Yoshi, Y. 2000, ApJ, 540, 81
- Trentham, N., Kormendy, J. K., & Sanders, D. B. 1999, AJ, 117, 2152 (TKS)
- Veilleux, S., Kim, D.-C., Sanders, D. B., Mazzarella, J. M., & Soifer, B. T. 1995, ApJS, 98, 171
- Veilleux, S., Kim, D.-C., and Sanders, D. B. 1999, ApJ, 522, 113
- Wade, R. A., Hoessel, J. G., Elias, J. H., & Huchra, J. P. 1979, PASP, 91, 35
- Williams, R., et al. 1996, AJ, 112, 1335
- Witt, A. N. & Gordon, K. D. 2000, ApJ, 528, 799
- Xia, X.-Y., Xue, S. J., Mao, S., Boller, Th., Deng, Z. G. & Wu, H. 2001, ApJ, in press
(astro-ph/0107559)
- Yun, M. S., Scoville, N. Z., & Knop, R. A. 1994, ApJ, 430, L109

Fig. 1.— We show the global relationship between UV color and FIR/UV fluxes. The line is a least-squares fit to the IUE starburst sample of M99 (the dots), and is consistent with a shell geometry for the dust distribution (Witt & Gordon 2000). Included are the three galaxies from TKS; β and IRX were computed in a manner similar to our own galaxies, taking into account the different wavelengths of their filters. Red leaks in the FOC near-UV filter may be partially responsible for the great redness of VII Zw 031. If that is true, then only the limit on the IRX (derived from the far-UV data) would be reliable.

Fig. 2.— The relationship between UV color and FIR/UV fluxes, in 2 kpc diameter apertures. The line is a simple foreground screen model fitted to the UV-selected starbursts. The IR fluxes in IRAS 08572+3915 and IRAS 19254–7245 have each been apportioned to 70% for the IR-bright nucleus and 30% for the IR-faint nucleus, as discussed earlier—note that these are conservative limits, and in both cases, the IR-bright nucleus may in fact produce essentially all the far-IR luminosity.

Fig. 3.— Far-UV, near-UV, and near-IR views of VV 114, 10 kpc on a side. The large tic marks are 1" apart.

Fig. 4.— The inner 3 kpc of VV 114 EAST in far-UV, near-UV, $F160W$, and 8.44 GHz. The crosses mark the positions of the 2.2 μm peaks, sources A and B of Doyon et al. (1995). The large tic marks are 1" apart.

Fig. 5.— The inner 3 kpc of VV 114 WEST at far-UV, near-UV, $F110W$, and $F160W$.

Fig. 6.— Far-UV, near-UV, optical, and near-IR views of IRAS 08572+3915, 20 kpc on a side. The large tic marks are 1" apart.

Fig. 7.— The inner 3 kpc of IRAS 08572+3915 NW in far-UV, near-UV, $F814W$, and $F160W$. The cross mark the position of the peak at 2.2 μm . The large tic marks are 1" apart.

Fig. 8.— The inner 3 kpc of IRAS 08572+3915 SE in far-UV, near-UV, $F814W$, and $F160W$. The cross mark the position of the peak at 2.2 μm . The large tic marks are 1" apart.

Fig. 9.— Far-UV, near-UV, and near-IR views of IC 883, 10 kpc on a side. The large tic marks are 1" apart.

Fig. 10.— The inner 3 kpc of IC 883 in far-UV, near-UV, $F110W$, and in the radio at 8.44 GHz. The large tic marks are 1" apart. The crosses mark the positions of the $F222M$ peaks (see text). Note that the astrometry is not sufficiently accurate to align the radio image with the HST images, so we have assumed that the brightest radio and 2.2 μm peaks are

coincident.

Fig. 11.— a) Far-UV, near-UV, optical, and near-IR views of Mrk 273, 10 kpc on a side. The large tic marks are 1" apart.

Fig. 12.— The inner 3 kpc of Mrk 273 in far-UV, near-UV, $F814W$, and $F160W$. The large tic marks are 1" apart. The crosses mark the positions of the radio/mid-IR peaks (see text).

Fig. 13.— Far-UV, near-UV, optical, and near-IR views of IRAS 15250+3609, 10 kpc on a side. The large tic marks are 1" apart.

Fig. 14.— The inner 3 kpc of IRAS 15250+3609 in far-UV, near-UV, $F814W$, and $F160W$. The cross marks the position of the peak at $2.2 \mu\text{m}$. The large tic marks are 1" apart.

Fig. 15.— a) Far-UV, near-UV, optical, and near-IR views of Arp 220, 10 kpc on a side. The large tic marks are 1" apart.

Fig. 16.— The inner 3 kpc of Arp 220 in far-UV, near-UV, $F814W$, and $F160W$. The large tic marks are 1" apart.

Fig. 17.— Far-UV, near-UV, and $F814W$ views of IRAS 19254–7245, with a $10 \text{kpc} \times 20 \text{kpc}$ field of view. The large tic marks are 1" apart. The crosses mark the positions of the brightest pixels in the $F814W$ image.

Fig. 18.— The inner 3 kpc of the northern and southern nuclei of IRAS 19254–7245 in far-UV, near-UV and $F814W$. The large tic marks are 1" apart. The crosses mark the positions of the nuclear peak pixels as measured in the $F814W$ image.

Fig. 19.— We show the growth curves of flux from our galaxies. The different point styles denote different nuclei. The horizontal dashed lines denote 100%, 50%, and 10% of the flux contained within the 5 kpc radius aperture. The curved dotted line shows the growth curve for a source with constant surface brightness. Arp 220 and IC 883, two galaxies without any strong sources in the inner kpc, are closest to the dotted line. IRAS 08572+3915 SE and IRAS 15250+3609, two galaxies that do have strong, centrally located sources, are farthest above the line, as would be expected. VV 114 E falls far below the line of constant surface brightness, as it emits virtually no near-UV light of its own, and its 5 kpc radius flux is almost entirely due to spillover from VV 114 W, part of which is included in the outer parts of the 5 kpc aperture centered on VV 114 E. The half-light radii in Table 4 were estimated using this figure.

Fig. 20.— We show the $F606W$ surface brightnesses of our galaxies, compared with the surface brightnesses of galaxies within the WF chips in the HDF, if our galaxies were placed at (a) $z = 1.54$; (b) $z = 3.12$. The symbols are the same as in Fig. 19.

Fig. 21.— We show the $V-I$ vs. V color-magnitude diagram of our galaxies, if located at $z = 3.12$, compared to the HDF U -band dropouts from M99. The symbols are the same as in Fig. 19.

Table 1. HST ULIG Sample and Physical Data^a

Galaxy (1)	redshift (z) (2)	Linear scale ^b (kpc/arcsec) (3)	Luminosity dist. ^b (Mpc) (4)	A_{FUV} (mag) (5)	$E(FUV - NUV)$ (mag) (6)	$\log(L_{IR}/L_\odot)$ (7)	FIR ^c (W m ⁻²) (8)
VV 114	0.0203	0.41	88.7	0.146	0.015	11.72	1.50×10^{-12}
IRAS 08572+3915	0.0583	1.13	260.4	0.245	0.023	12.17	5.60×10^{-13}
IC 883	0.0234	0.47	102.0	0.114	0.012	11.61	1.05×10^{-12}
Mrk 273	0.0382	0.76	168.2	0.076	0.008	12.17	1.43×10^{-12}
IRAS 15250+3609	0.0557	1.08	248.3	0.174	0.018	12.05	4.82×10^{-13}
Arp 220	0.0183	0.37	79.4	0.463	0.051	12.18	6.70×10^{-12}
IRAS 19254–7245	0.0611	1.18	273.4	0.785	0.085	12.10	3.51×10^{-13}

^aKeys to columns follow.

Col. 1—Sources, sorted in order of increasing Right Ascension.

Col. 2—redshift

Col. 3—Linear scale

Col. 4—Luminosity distance

Cols. 5–6—Milky Way far-UV extinction, and UV color excess, in magnitudes

Col. 7—Infrared luminosity

Col. 8—Far-IR flux

^bFor $H_0 = 70$ km/s/Mpc, $\Omega_M = 0.3$, and $\Omega_\Lambda = 0.7$

^cSources for the FIR data are: Soifer et al. (1989), and Sanders et al. (1995) (for IRAS 19254–7245 only).

Table 2. Log of HST ULIG Observations

Galaxy (1)	Obs. date (U.T.) (2)	FUV Exposure (sec) (3)	NUV Exposure (sec) (4)
VV 114	2000 Dec 25	3051	1500
IRAS 08572+3915	2000 Mar 1	3891	1500
IC 883	2000 Apr 5	3827	1500
Mrk 273	1999 May 13	3594	1500
IRAS 15250+3609	2000 May 27	3891	1500
Arp 220	2000 May 23	3749	1500
IRAS 19254–7245	1999 Aug 30	2829	1500

Table 3. HST ULIG Photometry^a

	Aperture radius					Total ^b
	0.5 kpc (1)	1 kpc (2)	2 kpc (3)	3 kpc (4)	5kpc (6)	
VV 114E						
	1''.210	2''.420	4''.840	7''.260	12''.100	Total ^b
FUV	22.70	21.08	19.21	17.70	15.60	14.73
unc.	0.23	0.21	0.15	0.08	0.03	0.02
NUV	22.10	20.39	18.38	17.00	15.08	14.26
unc.	0.09	0.07	0.04	0.03	0.01	0.01
β	-1.12	-0.93	-0.67	-0.92	-1.25	-1.35
unc.	0.46	0.41	0.29	0.16	0.07	0.04
log(IRX)	4.10	3.45	2.71	2.11	1.27	1.13
VV 114W						
	1''.210	2''.420	4''.840	7''.260	12''.100	Total ^b
FUV	17.70	16.58	15.71	14.98	14.78	...
unc.	0.01	0.01	0.01	0.01	0.02	...
NUV	17.14	16.02	15.20	14.53	14.29	...
unc.	0.01	0.01	0.01	0.01	0.01	...
β	-1.18	-1.18	-1.28	-1.39	-1.33	...
unc.	0.01	0.01	0.01	0.01	0.03	...
log(IRX)	1.92	1.48	1.13	0.84	0.76	...
IRAS 08572+3915NW						
	0''.444	0''.887	1''.774	2''.661	4''.435	Total ^b
FUV	25.90	23.60	22.02	21.21	20.39	19.24
unc.	0.33	0.16	0.14	0.15	0.20	0.27
NUV	24.88	22.52	21.08	20.41	19.82	18.99
unc.	0.21	0.10	0.10	0.12	0.20	0.18
β	-0.31	-0.21	-0.47	-0.72	-1.16	-0.66
unc.	0.74	0.34	0.33	0.37	0.53	0.61
log(IRX)	4.98	4.06	3.43	3.11	2.78	2.47
IRAS 08572+3915SE						
	0''.444	0''.887	1''.774	2''.661	4''.435	Total ^b
FUV	22.15	21.67	21.14	20.74	19.91	...
unc.	0.02	0.03	0.06	0.10	0.13	...
NUV	21.41	21.01	20.64	20.44	19.82	...

Table 3—Continued

	0.5 kpc (1)	Aperture radius					Total ^b (7)
		1 kpc (2)	2 kpc (3)	3 kpc (4)	5kpc (5)	6	
unc.	0.01	0.03	0.07	0.13	0.20	...	
β	-0.85	-1.01	-1.31	-1.66	-2.07	...	
unc.	0.04	0.07	0.18	0.30	0.45	...	
log(IRX)	3.12	2.92	2.71	2.55	2.22		

IC 883						
	1''059	2''117	4''235	6''352	10''587	Total ^b
FUV	22.82	21.26	19.80	19.12	18.58	18.45
unc.	0.09	0.09	0.09	0.11	0.18	0.16
NUV	21.72	20.15	18.75	18.14	17.71	17.61
unc.	0.04	0.04	0.04	0.05	0.10	0.15
β	-0.17	-0.14	-0.25	-0.39	-0.58	-0.64
unc.	0.19	0.18	0.18	0.22	0.39	0.41
log(IRX)	4.23	3.61	3.02	2.75	2.54	2.48

Mrk 273						
	0''661	1''322	2''644	3''966	6''610	Total ^b
FUV	22.37	21.39	20.48	19.79	19.00	18.66
unc.	0.02	0.03	0.05	0.07	0.09	0.12
NUV	20.84	19.81	19.07	18.56	17.96	17.78
unc.	0.01	0.02	0.03	0.05	0.08	0.13
β	0.65	0.76	0.43	0.10	-0.26	-0.56
unc.	0.05	0.07	0.12	0.15	0.22	0.33
log(IRX)	4.20	3.81	3.44	3.17	2.85	2.71

IRAS 15250+3609						
	0''.463	0''.926	1''.852	2''.778	4''.630	Total ^b
FUV	21.81	19.88	19.30	19.07	18.93	18.73
unc.	0.01	0.01	0.01	0.02	0.05	0.10
NUV	20.85	19.03	18.47	18.23	18.11	18.01
unc.	0.01	0.01	0.01	0.01	0.03	0.06
β	-0.43	-0.63	-0.68	-0.67	-0.71	-0.87
unc.	0.03	0.01	0.03	0.05	0.11	0.22
log(IRX)	3.47	2.69	2.46	2.37	2.31	2.23

Table 3—Continued

(1)	Aperture radius					Total ^b (7)
	0.5 kpc (2)	1 kpc (3)	2 kpc (4)	3 kpc (5)	5kpc (6)	
	1.''346	2.''692	5.''384	8.''076	13.''460	
FUV	24.30	22.83	21.03	20.08	19.73	19.68
unc.	0.47	0.49	0.37	0.35	0.69	0.31
NUV	23.84	22.41	20.30	19.22	18.52	18.51
unc.	0.46	0.50	0.28	0.24	0.35	0.14
β	-1.44	-1.51	-0.94	-0.67	-0.04	-0.09
unc.	1.24	1.30	0.87	0.79	1.45	0.64
log(IRX)	5.49	4.9	4.18	3.80	3.66	3.64
IRAS 19254–7245N						
	0.''425	0.''849	1.''698	2.''547	4.''245	Total ^b
FUV	25.43	24.08	23.14	22.31	21.44	...
unc.	0.12	0.12	0.20	0.21	0.26	...
NUV	23.70	22.72	22.10	21.56	20.85	...
unc.	0.07	0.11	0.23	0.32	0.46	...
β	0.89	0.19	-0.40	-0.95	-1.25	...
unc.	0.27	0.31	0.58	0.72	1.00	...
log(IRX)	4.01	3.47	3.09	2.76	2.41	
IRAS 19254–7245S						
	0.''425	0.''849	1.''698	2.''547	4.''245	Total ^b
FUV	>27.24	>25.73	23.87	22.60	21.74	20.31
unc.	0.39	0.27	0.34	0.25
NUV	23.64	23.17	22.20	21.34	20.59	19.58
unc.	0.07	0.16	0.26	0.26	0.36	0.44
β	> 4.41	> 3.38	0.77	0.00	-0.20	-0.98
unc.	0.88	0.71	0.94	0.95
log(IRX)	> 5.10	> 4.70	3.75	3.25	2.90	2.48

^aPhotometry is given in the AB magnitude system. Upper limits are 2σ .

^bQuantities include the contributions from both components of the system.

Table 4. Predictions for detecting ULIGs in the HDF

Galaxy (1)	$R_{0.5}$ (kpc) (2)	Surface brightness ($F606W_{AB}$)	
		$z = 1.54$ (Mag/arcsec 2) (3)	$z = 3.12$ (Mag/arcsec 2) (4)
VV 114 E	4	24.84	26.93
VV 114 W	2.25	22.81	24.85
IRAS 08572+3915NW	2.75	26.37	28.50
IRAS 08572+3915SE	2.25	25.94	27.59
IC 883	2.75	26.39	28.82
Mrk 273	2.75	25.60	28.21
IR 15250+3609	1.25	23.13	25.49
Arp 220	3	27.62	30.35
IR 19254–7245N	3	27.02	29.10
IR 19254–7245S	3	26.76	29.39

Table 5. Absolute Far-UV magnitudes for ULIGs^a

Galaxy (1)	M_{FUV} (MW ext. only) ^b (Mag.) (2)	M_{FUV} (MW+Int. ext.) ^b (Mag) (3)
VV 114 E	−19.27	−21.2
VV 114 W	−20.09	−21.8
IRAS 08572+3915NW	−16.88	−19.0
IRAS 08572+3915SE	−17.36	−17.7
IC 883	−16.54	−19.7
Mrk 273	−17.17	−21.1
IR 15250+3609	−18.15	−21.2
Arp 220	−15.21	−19.5
IR 19254−7245N	−16.47	−18.4
IR 19254−7245S	−16.17	−20.2

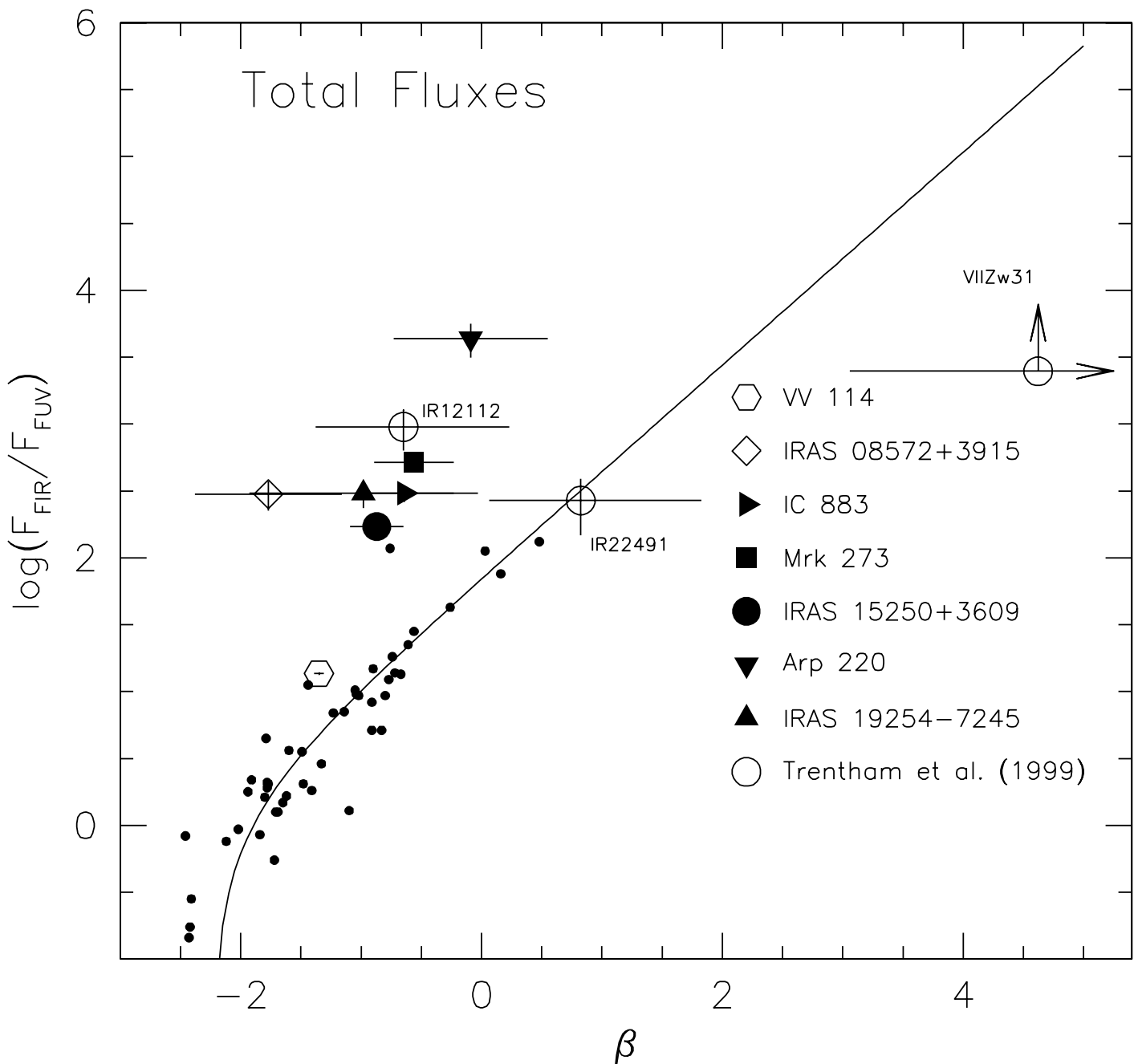
^aUV photometry is in 5 kpc physical apertures. Photometry is given in the AB system.

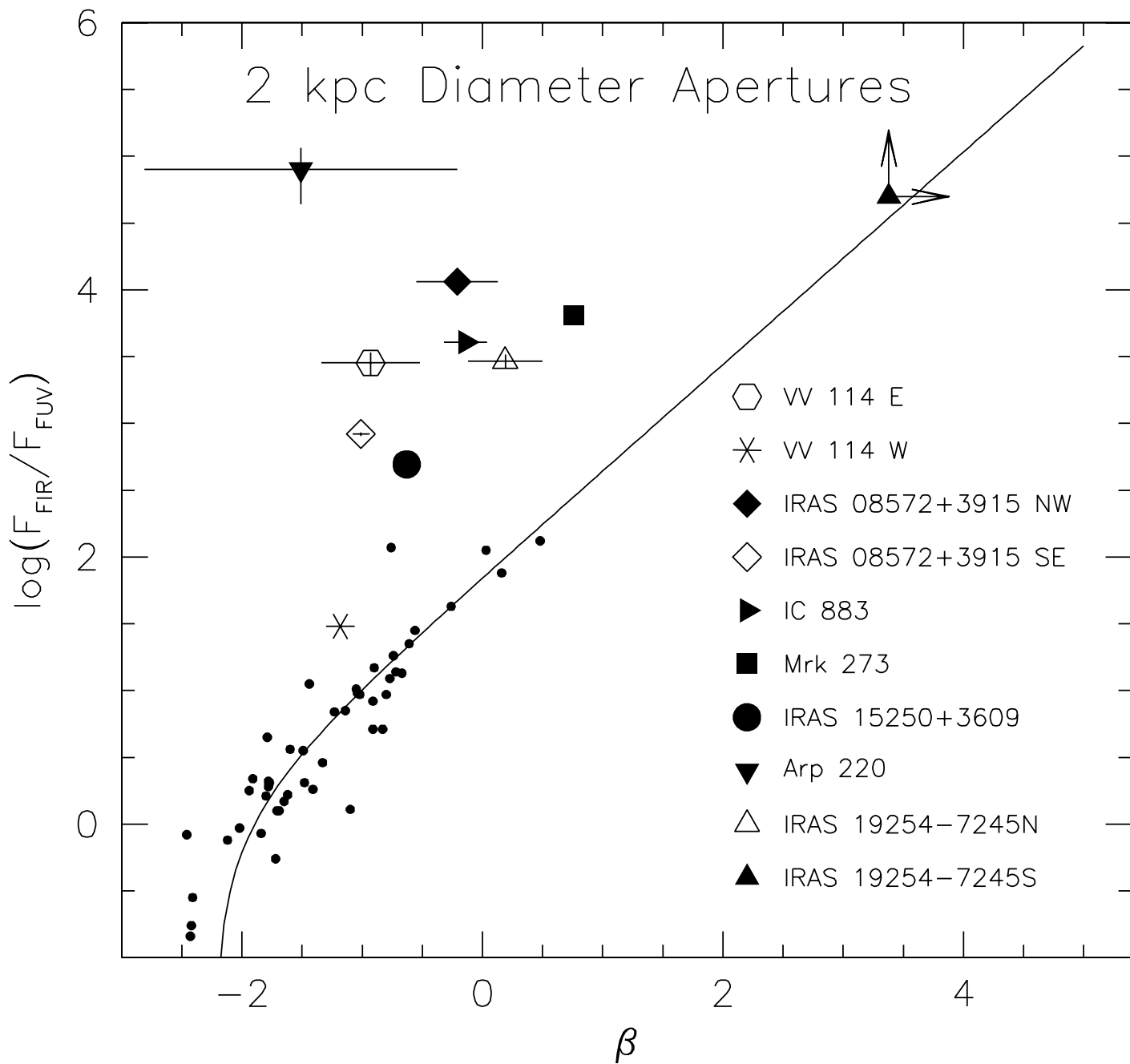
^bColumn (2) gives absolute magnitudes corrected for foreground (Milky Way) extinction only. Column (3) also includes a correction for internal extinction, $A_{FUV} \approx 4.4 + 2\beta$, taken from M99.

Table 6. Predicted colors for ULIGs at high redshifts^a

Galaxy	At $z = 1.96$			At $z = 3.80$		
	R (Mag)	K (Mag)	$R - K$ (Mag)	R (Mag)	K (Mag)	$R - K$ (Mag)
(1)	(2)	(3)	(4)	(5)	(6)	(7)
IRAS 08572+3915NW	27.01	20.82	6.19	28.78	23.11	5.67
Mrk 273	26.24	21.59	4.65	28.49	23.61	4.88
IRAS 15250+3609	25.48	22.33	3.15	27.48	24.12	2.66
Arp 220	28.07	22.52	5.55	30.44	24.49	5.95
IRAS 19254–7245S	27.21	21.69	5.52	29.48	24.10	5.38

^aPredicted using UV photometry is in 5 kpc physical apertures, and optical photometry through 10'' diameter apertures, except for IRAS 19254–7245 (8'' optical). Photometry is given in the Johnson system in this table only.





This figure "figure-3.jpg" is available in "jpg" format from:

<http://arXiv.org/ps/astro-ph/0112352v1>

This figure "figure-4.jpg" is available in "jpg" format from:

<http://arXiv.org/ps/astro-ph/0112352v1>

This figure "figure-5.jpg" is available in "jpg" format from:

<http://arXiv.org/ps/astro-ph/0112352v1>

This figure "figure-6.jpg" is available in "jpg" format from:

<http://arXiv.org/ps/astro-ph/0112352v1>

This figure "figure-7.jpg" is available in "jpg" format from:

<http://arXiv.org/ps/astro-ph/0112352v1>

This figure "figure-8.jpg" is available in "jpg" format from:

<http://arXiv.org/ps/astro-ph/0112352v1>

This figure "figure-9.jpg" is available in "jpg" format from:

<http://arXiv.org/ps/astro-ph/0112352v1>

This figure "figure-10.jpg" is available in "jpg" format from:

<http://arXiv.org/ps/astro-ph/0112352v1>

This figure "figure-11.jpg" is available in "jpg" format from:

<http://arXiv.org/ps/astro-ph/0112352v1>

This figure "figure-12.jpg" is available in "jpg" format from:

<http://arXiv.org/ps/astro-ph/0112352v1>

This figure "figure-13.jpg" is available in "jpg" format from:

<http://arXiv.org/ps/astro-ph/0112352v1>

This figure "figure-14.jpg" is available in "jpg" format from:

<http://arXiv.org/ps/astro-ph/0112352v1>

This figure "figure-15.jpg" is available in "jpg" format from:

<http://arXiv.org/ps/astro-ph/0112352v1>

This figure "figure-16.jpg" is available in "jpg" format from:

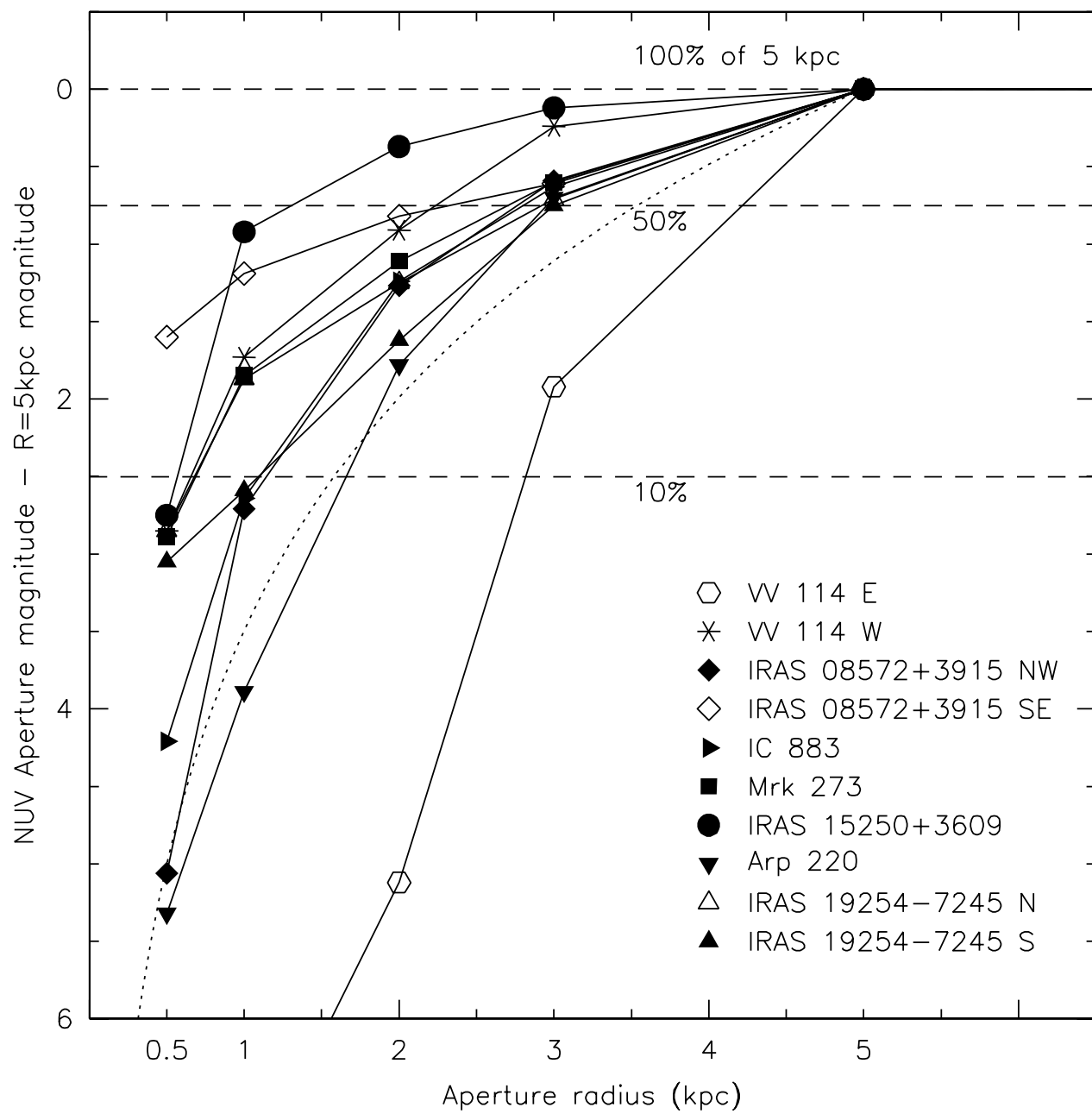
<http://arXiv.org/ps/astro-ph/0112352v1>

This figure "figure-17.jpg" is available in "jpg" format from:

<http://arXiv.org/ps/astro-ph/0112352v1>

This figure "figure-18.jpg" is available in "jpg" format from:

<http://arXiv.org/ps/astro-ph/0112352v1>



This figure "figure-20a.jpg" is available in "jpg" format from:

<http://arXiv.org/ps/astro-ph/0112352v1>

This figure "figure-20b.jpg" is available in "jpg" format from:

<http://arXiv.org/ps/astro-ph/0112352v1>

This figure "figure-21.jpg" is available in "jpg" format from:

<http://arXiv.org/ps/astro-ph/0112352v1>